NOAA Technical Memorandum NWS TDL 76

THE APPLICATION OF CUMULUS MODELS TO MOS FORECASTS OF CONVECTIVE WEATHER

Techniques Development Laboratory
Silver Spring, MD
June 1985

U.S. DEPARTMENT OF COMMERCE / National Ocean and Atmospheric Administration / National Weather Service

NOAA TECHNICAL MEMORANDUMS

National Weather Service, Techniques Development Laboratory Series

The primary purpose of the Techniques Development Laboratory of the Office of Systems Development is to translate increases of basic knowledge in meteorology and allied disciplines into improved operating techniques and procedures. To achieve this goal, the Laboratory conducts applied research and development aimed at the improvement of diagnostic and prognostic methods for producing weather information. The Laboratory performs studies both for the general improvement of prediction methodology used in the National Meteorological Service and for the more effective utilization of weather forecasts by the ultimate user.

NOAA Technical Memorandums in the National Weather Service Techniques Development Laboratory series facilitate rapid distribution of material that may be preliminary in nature and which may be published formally elsewhere at a later date. Publications 1 through 5 are in the former series Weather Bureau Technical Notes (TN), Techniques Development Laboratory (TDL) Reports; publications 6 through 36 are in the former series ESSA Technical Memorandums, Weather Bureau Technical Memorandum, (WBTM). Beginning with TDL 37, publications are now part of the series NOAA Technical Memorandums, National Weather Service (NWS).

Publications listed below are available from the National Technical Information Service, U.S. Department of Commerce, Sills Bldg., 5285 Port Royal Road, Springfield, VA 22161. Prices on request. Order by accession number (given in parentheses).

ESSA Technical Memorandums

WBTM TDL 17 Second Interim Report on Sea and Swell Forecasting. N. A. Pore and W. S. Richardson, January 1969, 7 pp. plus 10 figures. (PB-182-273)

WBTM TDL 18 Conditional Probabilities of Precipitation Amounts in the Conterminous United States. Donald L. Jorgensen, William H. Klein, and Charles F. Roberts, March 1969, 89 pp. (PB-183-144)

WBTM TDL 19 An Operationally Oriented Small-Scale 500-Millibar Height Analysis Program. Harry R. Glahn and George W. Hollenbaugh, March 1969, 17 pp. (PB-184-111)

WBTM TDL 20 A Comparison of Two Methods of Reducing Truncation Error. Robert J. Bermowitz, May 1969, 7 pp. (PB-184-741)

WBTM TDL 21 Automatic Decoding of Hourly Weather Reports. George W. Hollenbaugh, Harry R. Glahn, and Dale A. Lowry, July 1969, 27 pp. (PB-185-806)

WBTM TDL 22 An Operationally Oriented Objective Analysis Program. Harry R. Glahn, George W. Hollenbaugh, and Dale A. Lowry, July 1969, 20 pp. (PB-186-129)

WBTM TDL 23 An Operational Subsynoptic Advection Model. Harry R. Glahn, Dale A. Lowry, and George W. Hollenbaugh, July 1969, 26 pp. (PB-186-389)

WBTM TDL 24 A Lake Erie Storm Surge Forecasting Technique. William S. Richardson and N. Arthur Pore, August 1969, 23 pp. (PB-185-778)

WBTM TDL 25 Charts Giving Station Precipitation in the Plateau States From 850- and 500-Millibar Lows During Winter. August F. Korte, Donald L. Jorgensen, and William H. Klein, September 1969, 9 pp. plus appendixes A and B. (PB-187-476)

WBTM TDL 26 Computer Forecasts of Maximum and Minimum Surface Temperatures. William H. Klein, Frank Lewis, and George P. Casely, October 1969, 27 pp. plus appendix. (PB-189-105)

WBTM TDL 27 An Operational Method for Objectively Forecasting Probability of Precipitation. Harry R. Glahn and Dale A. Lowry, October 1969, 24 pp. (PB-188-660)

WBTM TDL 28 Techniques for Forecasting Low Water Occurrence at Baltimore and Norfolk. James M. McClelland, March 1970, 34 pp. (PB-191-744)

WBTM TDL 29 A Method for Predicting Surface Winds. Harry R. Glahn, March 1970, 18 pp. (PB-191-745)

WBTM TDL 30 Summary of Selected Reference Material on the Oceanographic Phenomena of Tides, Storm Surges, Waves, and Breakers. N. Arthur Pore, May 1970, 103 pp. (PB-193-449)

WBTM TDL 31 Persistence of Precipitation at 108 Cities in the Conterminous United States. Donald L. Jorgensen and William H. Klein, May 1970, 84 pp. (PB-193-599)

WBTM TDL 32 Computer-Produced Worded Forecasts. Harry R. Glahn, June 1970, 8 pp. (PB-194-262)

WBTM TDL 33 Calculation of Precipitable Water. L. P. Harrison, June 1970, 61 pp. (PB-193-600)

WBTM TDL 34 An Objective Method for Forecasting Winds Over Lake Erie and Lake Ontario. Celso S. Barrientos. August 1970, 20 pp. (PB-194-586)

WBTM TDL 35 Probabilistic Prediction in Meteorology; a Bibliography. Allan H. Murphy and Roger A. Allen, June 1970, 60 pp. (PB-194-415)

WBTM TDL 36 Current High Altitude Observations--Investigation and Possible Improvement. M. A. Alaka and R. C. Elvander, July 1970, 24 pp. (COM-71-00003)

NWS TDL 37 Prediction of Surface Dew Point Temperatures. R. C. Elvander, February 1971, 40 pp. (COM-71-00253)

NWS TDL 38 Objectively Computed Surface Diagnostic Fields. Robert J. Bermowitz, February 1971, 23 pp. (COM-71-0301)

NWS TDL 39 Computer Prediction of Precipitation Probability for 108 Cities in the United States. William H. Klein, February 1971, 32 pp. (COM-71-00249)

NWS TDL 40 Wave Climatology for the Great Lakes. N. A. Pore, J. M. McClelland, C. S. Barrientos, and W. E. Kennedy, February 1971, 61 pp. (COM-71-00368)

NWS TDL 41 Twice-Daily Mean Heights in the Troposphere Over North America and Vicinity. August F. Korte, June 1971, 31 pp. (COM-71-0286)

(Continued on inside back cover)

NOAA Technical Memorandum NWS TDL 76

THE APPLICATION OF CUMULUS MODELS TO MOS FORECASTS OF CONVECTIVE WEATHER

David H. Kitzmiller

Techniques Development Laboratory
Silver Spring, MD

June 1985

UNITED STATES DEPARTMENT OF COMMERCE
Malcolm Baldrige, Secretary

National Oceanic and Atmospheric Administration
Anthony J. Calio,
Deputy Administrator

National Weather Service
Richard E. Hallgren,
Assistant Administrator

Table of Contents

THE APPLICATION OF CUMULUS MODELS TO MOS FORECASTS OF CONVECTIVE WEATHER

David H. Kitzmiller

ABSTRACT

The National Weather Service currently issues twice-daily forecasts of thunderstorm and severe local storm probability based on Model Output Statistics. The probability forecasts are given by a weighted linear combination of meteorological predictors derived from NMC's limited-area fine mesh (LFM) model and TDL's three-dimensional trajectory model.

In the current system, model predictors such as the K index and 1000-mb heights do not explicitly include the effects of convection processes. In an effort to improve the resolution of forecasts, new predictors derived from models of cumulus dynamics and thermodynamics have been developed and tested. The cumulus models and associated predictors add new information by emphasizing the subgrid, cloud-scale processes important in the development of thunderstorms. In addition, the impact of predictors derived from a boundary-layer model of significantly greater spatial resolution than the LFM model has been examined. This boundary-layer model has been run in a quasi-operational mode by TDL since 1978, resulting in a stable long-period data sample for MOS development.

Two cumulus model predictors, a rainfall parameter and the maximum updraft speed, were found to be highly correlated to general thunderstorm and severe local storm occurrence, respectively, In addition, the use of forecast data from the boundary-layer model leads to a further increase in the correlation between the predictors and general thunderstorm activity.

A multiple linear screening regression procedure was used to derive new probability equations that utilize both the experimental and operational predictors. Probability forecasts for independent cases were then derived from these equations. The bias or reliability of these forecasts was found to be comparable to that of the current operational forecasts. For both thunderstorms and severe local storms, the experimental forecasts gave higher scores in terms of probability of detection and critical success index.

1. INTRODUCTION

Since 1977, the National Weather Service has issued daily forecasts of thunderstorm and severe local storm probability based on Model Output Statistics (MOS). The probability forecasts are given by a weighted linear combination of meteorological predictors obtained from the National Meteorological Center's limited-area fine mesh (LFM) model (Gerrity, 1977) and from the Techniques Development Laboratory's (TDL's) three-dimensional trajectory model (Reap, 1972). The probability forecast equation for thunderstorms is based on the long-term statistical relationships between the model predictors and radar observations of thunderstorm phenomena. Forecast equations for severe local storms are based upon actual reports of tornadoes, large hail, and damaging winds. Reap and Foster (1979) describe the procedures used in deriving these probability equations.

The most important predictors in the current operational forecast equations, such as the K index, Total Totals index, and 1000-mb heights, are not based on explicit physical models of convection processes. In an effort to further refine the probability forecasts, we have derived several new predictors from models of cumulus dynamics and thermodynamics. The use of such models in deriving predictors adds new information by emphasizing the physical processes important in thunderstorm development. These predictors indicate the potential for deep cumulus cloud development and the strength of convective circulations. In the course of this study, we also employed forecast data from TDL's boundary-layer model (Long et al., 1978), which has higher spatial resolution than does the LFM. The boundary-layer model (BLM) has been run operationally since 1978, providing a stable, long-period data sample for use in MOS development.

In order to illustrate some of the characteristics of the new predictors, we will present two cases showing the manner in which the spatial and temporal distribution of the predictors reflects observed thunderstorm events, and the results of statistical comparisons that demonstrate the predictors' ability to forecast such events.

2. CUMULUS CLOUD MODEL

To estimate convective cloud properties, we analyze the temperature and moisture profiles forecast by large-scale numerical models with a simple entraining jet cloud model (for a complete explanation of the cloud model, see Appendix). This cloud model was developed by Weinstein and Davis (1968). Many investigators have used the model for simulating the development of cumuli and thunderstorms (see, for example, Simpson and Wiggert, 1969, Sanders and Garrett, 1975, and Crum and Cahir, 1983). In an earlier study, Kreitzberg et al. (1978) attempted to predict precipitation occurrence and amount using forecasts from a cumulus convection model and from the LFM. Though they found that the addition of information from the cumulus model had little positive impact on the forecasts, the prediction problem that they undertook was substantially different from ours. Their quantitative precipitation forecasts were verified against single rainguage measurements. Such observations are highly variable in space even when taken over 6-h or 12-h time intervals, making the prediction problem very difficult. Since virtually any prediction scheme would show little skill in forecasting point precipitation amounts, it is difficult to relate

their results to the present study. Their precipitation occurrence forecasts were verified against both surface observations and Manually-Digitized Radar (MDR) reports. The MDR data were digitized on a grid with elements approximately one fourth the size of the elements in our study's verification grid, and the verification periods were shorter than in our study. Though most of their results were negative, they did find that the cumulus model added some skill beyond the LFM in the forecasting precipitation occurrence indicated by radar echoes.

The quasi-Langrangian cloud model employed in this study is based on the integration of a vertical motion equation that forecasts the cloud updraft speed at successively higher levels. It features a lateral entrainment rate inversely proportional to the updraft radius and simple liquid-phase microphysics that determine the amount of rain produced by the cloud. The analysis yields maximum updraft speed in the cloud (WMX), cloud depth (H), and a rainout term (RN). We define RN as the depth of rainwater released from a parcel within the cloud during the time it takes the parcel to ascend from cloud base to top. RN is determined from the microphysical equations and is roughly proportional to the cloud depth and the low-level moisture supply. The cloud depth H is defined as the pressure difference between cloud base and cloud top. We define WMX as the largest vertical velocity within the cloud.

The cloud model analysis is obtained in the following manner. After the temperature and moisture profiles have been constructed from the archive forecasts, the cloud condensation level is determined. This is the lifting condensation level for an air parcel having the mean mixing ratio of the lowest 100 mb of the profile. (See Stone, 1983 for the details of this computation). The model updraft begins at this level, where it is assumed to be saturated and have the same temperature as its surroundings. The initial updraft speed is taken to be 1 m s^{-1}; the updraft radius is set at 500 m, corresponding to a lateral entrainment rate of 0.4 km^{-1}. The cloud top is taken to be the level at which the updraft speed vanishes.

Another predictor derived from BLM and LFM data provides a measure of convective available potential energy within the forecast profile. This predictor (B) is defined as:

$$B = \int_{z_b}^{z_t} \frac{(T' - T)}{T} \, dz$$

where T' is the temperature within an enclosed parcel undergoing pseudo-adiabatic ascent, T is the temperature within the large-scale environment at the same level, z_b is the height of the lifting condensation level and z_t is the top of the first positive energy area encountered during ascent. In addition, we compute a combined predictor MB by multiplying B by the boundary-layer moisture convergence M where $M = -\nabla \cdot \underline{V}.q$. The predictor MB reflects the magnitude of conditional instability and low-level convergence; both conditions must be present in order for thunderstorms to occur.

Another predictor based on a physical model of convection, the "best" lifted index (BLI), is described by Shaffer et al. (1979). This quantity gives the most unstable value of the lifted indices computed from four different layers within the BLM domain. These are the lowest three 50-mb layers and the lowest 100-mb layer. The LFM forecast provides the 500-mb temperature for the calculation. Shaffer et al. (1979) found that this predictor, when considered simultaneously with the BLM's moisture convergence forecast, is a reasonably accurate indicator of severe local storm potential. The complete list of experimental and operational predictors that were submitted to the screening regression process to derive new forecast equations is given in Table 1.

Plots of the observed relative 12-36 h frequency of predictand versus predictor variables often show that the relationship between predictor and predictand is highly nonlinear. The relationship between general thunderstorm frequency and the 24-h LFM rainout forecast is nonlinear (see Fig. 1), while the relationship between observed severe thunderstorm frequency and the same predictand is nearly linear. In the nonlinear cases, the linear regression model would most likely not select such predictors because of a failure to adequately represent the true relationship.

To overcome this difficulty, the predictor variables were transformed to insure a linear relationship to the predictand relative frequency. For example, to linearize the rainout predictor mentioned earlier, we transformed the original predictor to the corresponding event frequency by fitting a low-order polynomial to the frequency curve. This process can substantially increase the linear correlation between the predictor and the predictand and result in the selection of a predictor that was formerly rejected by the regression procedure.

3. PREDICTOR DATA

In order to test the impact of the high-resolution BLM forecasts, we derived most of the experimental predictors described in the previous section both from LFM data alone and from a combination of BLM and LFM data. Fig. 2 shows the BLM's forecast domain. The model's computational mesh, about 84 km, is significantly smaller than that of the LFM. In addition, the BLM contains ten vertical layers, with the lowest at the surface and the highest at 2000 m local height. Though the LFM provides time tendencies for variables at the BLM's upper boundary, the BLM has a separate analysis and initialization. See Long et al. (1978) for further details.

All of the cloud model predictors and the potential energy predictor B described in the previous section can be computed from either an LFM forecast alone or from a combination of BLM forecast data in the lowest two kilometers and LFM data above that level. We used LFM forecasts for the surface and for the 850-, 700-, 500-, 400-, 300-, and 200-mb levels. When BLM data were included, we used the forecasts for the surface and for the 305-, 610-, 990-, 1410-, and 2000-m levels, and the LFM forecasts for information at 500 mb and above. In this study, all predictors were derived for 24-h projections from forecast model runs started with 0000 GMT initial data. Experience has shown that predictors at this time projection are the most important in forecasting thunderstorm events during the 12-36 h period.

4. PREDICTAND DATA SAMPLE

Our predictand sample consists of radar data and severe storm reports for 624 days from 15 March to 15 September during the years 1980-1983. The predictand data for severe storms consists of reports of tornadoes, hail larger than 2 cm in diameter, and wind gusts greater than 93 km h^{-1} or wind damage. These reports were extracted from tapes edited and prepared at the National Severe Storms Forecast Center.

The predictand data for general thunderstorm activity consists of Manually-Digitized Radar (MDR) reports archived at TDL (Foster and Reap, 1978). These data are tabulated for geographical blocks about 75-80 km on a side; the predictand sample covers most of the United States east of the Rocky Mountains. In this study, we assumed that a thunderstorm occurred within the grid block if a level 3 or higher echo was observed by the Video Integrator and Processor (VIP) which is an adjunct to the operational WSR-57 network radars. Reap and Foster (1979) showed this to be a reliable criterion for thunderstorm occurrence.

5. SEVERE LOCAL STORM CASE STUDIES

We will present two cases illustrating the correspondence between the experimental predictors and significant thunderstorm and severe thunderstorm activity. The cases will also demonstrate the impact of high-resolution BLM data on the predictor fields. The predictors are 24-h forecasts derived from BLM and LFM model runs based on 0000 GMT initial data. Details concerning the severe storm reports were obtained from Storm Data (NOAA, 1983). Radar reports were extracted from TDL's extensive archive of MDR data. Though all of the convective predictors require LFM data as input, for the sake of simplicity we refer to the predictors derived from LFM data alone as "LFM" predictors and to those derived from BLM and LFM data as "BLM" predictors. In the latter case, LFM data are used above the 2000-m level, which is the top of the BLM domain.

The first case concerns the severe weather around 0000 GMT on 3 May 1983. At 1200 GMT on 2 May, a deep occluded low pressure system was centered over Lake Superior. An attendant cold front extended from Michigan to Texas, with the southern portion moving rapidly eastward. With much warm, moist air ahead of the front, severe thunderstorms appeared possible anywhere along its length. Temperatures in the upper Midwest rose to the 70's during the day, and hail, high winds, and some tornadoes broke out in Ohio, Michigan, Pennsylvania, and New York (Fig. 3). Radar reports (Fig. 4) at 0000 GMT on 3 May showed extensive thunderstorm activity along an axis from Arkansas to Pennsylvania.

The numerical models indicated intense convection on this day. The BLI (Fig. 5) showed an unstable area over New York and Pennsylvania, with some indices as large as -6K over Pennsylvania. According to Shaffer et al. (1979), the region of severe storm potential is best defined as that in which the BLI is < -2K and the low-level moisture convergence is > 1 g kg^{-1} h^{-1}. This area is shown by the dashed line in Fig. 5.

Figs. 6 and 7 show the cloud depth H, which we previously defined as the difference in pressure between cloud base and cloud top. This parameter indicates the depth of the layer favorable to convection. The field shows good general correspondence to the observed intense radar echoes, with the largest values over the Midwest through the Mississippi Valley. The BLM has clouds nearly 400 mb deep over Ohio, while the LFM shows clouds nearly 500 mb deep over Arkansas.

The convective vertical velocity, WMX, appear in Figs. 8 and 9. This quantity indicates the amount of kinetic energy that can be released by convective overturning. The BLM's WMX tends to be larger than the LFM's, probably because of surface temperatures forecast by the BLM. The BLM predictor reflects the area of radar echoes more closely than the LFM WMX forecast.

The rainout term RN (Figs. 10 and 11) provides a measure of both the depth of the unstable layer and the amount of low-level moisture. Data from the BLM forecast had a strong impact on the geographical distribution of this term. In the LFM forecast, the deep clouds over Arkansas had nearly 10 mm of rainout, while less than 1 mm was indicated for the clouds over the Midwest (a small local maximum appears over Ontario). However, the BLM forecast had two significant maxima, the greater over Ohio and Pennsylvania. The different moisture distribution in the BLM plays a large role in creating such differences.

The available potential energy term B, shown in Figs. 12 and 13, reflects both the depth of the unstable layer and the magnitude of the temperature excess within convectively ascending air. Because it is proportional to the geometric depth of the unstable layer, the parameter is large where the atmosphere is warmest. Thus, B reaches high values over Texas even though the most intense convection indicated by the cloud model occurs elsewhere. A secondary maximum is found over the unstable region in the Midwest.

On the following day (the second in our case study), thunderstorms were less widespread, and only a few severe storms were reported. By 1200 GMT on 3 May, the deep upper-air low over the Great Lakes had weakened and begun to move northeastward. A rapidly-moving cold front extending from Ohio to Alabama dominated the weather over the eastern states on this day. Warm, humid air covered the region over and east of the Appalachians, so strong thunderstorms again seemed likely (see the MOS forecast, Fig. 14). However, almost no severe weather developed (the storms over Louisiana occurred about 1400 GMT on the morning of 3 May). Thunderstorm activity as indicated by radar (Fig. 15) was much less extensive than on the previous evening.

Though the MOS forecast showed fairly large storm probabilities, convective activity forecast by the models promised to be weak (see Figs. 16-24). No lifted indices (Fig. 16) were lower than -1K, though strong moisture convergence (not shown) took place along the Appalachians ahead of the cold front. Virtually all of the convection indices are considerably smaller than in the previous day's forecasts. The BLM's vertical velocity field (Fig. 19) has values in excess of 15 m s^{-1}, probably reflecting some instability in a shallow layer. The BLM also forecast some clouds deeper than 300 mb over New York, at the northern edge of the model grid. This area might correspond to the observed region of VIP3 radar echoes (Fig. 15).

In the two cases shown, the convective cloud properties derived from model forecasts had good spatial correlation to convective activity indicated by radar. The magnitudes of most of the predictors decreased markedly from the first to the second case, as did the extent and intensity of the observed thunderstorms. The cloud depth (H) and updraft speed (WMX) predictors tended to be largest in the vicinity of reported severe storms. Information from the boundary-layer model clearly influenced some of the derived cloud properties (see, for example, Figs. 10 and 11).

On the basis of these and other case studies, we decided that the experimental predictors were good candidates for submission to the screening regression procedure from which probability forecast equations were derived.

6. GENERAL THUNDERSTORM PROBABILITY EQUATION

Using the multiple screening regression procedure described by Glahn and Lowry (1972), we derived experimental equations for the probability of thunderstorms during the period 12-36 h after 0000 GMT initial time. This procedure uses an algorithm to select a weighted linear combination of predictors that explains the greatest amount of the given predictand's variance. In the experiments described here, we submitted the current operational predictors and all of the experimental ones to the regression procedure at the same time.

The correlation statistics shown below were derived from a predictor/predictand sample covering the period 15 March to 15 September for the years 1980-83. When missing forecasts are taken into account, the sample consists of a total of 624 days. The predictors were computed for each of 714 verification grid blocks, each containing about 6400 km^2, over the United States east of the Rocky Mountains. The thunderstorm predictand is binary; it is 1 if a radar echo of VIP3 intensity or greater was observed within the grid block during 12-36 h the period, and 0 otherwise.

Table 2 shows linear correlation coefficients between thunderstorm events and both operational and experimental predictors. The K index (Miller, 1972) consistently shows very high correlation to general thunderstorm activity. The product of K and the climatological frequency F, denoted KF*, forms the basis for the most important predictor in the current operational equation (see Reap and Foster, 1979). We derived an alternative version of the K index by using the BLM forecast to provide the 850-mb temperature and dewpoint. Among the nonlinearized predictors, the updraft speed WMX and cloud depth H are most highly correlated; apparently the degree of instability and the depth of the unstable layer are very important in determining the likelihood of thunderstorms. The relationship between the rainout term RN and event frequency is highly nonlinear; linearizing the predictor makes it the most highly-correlated. The introduction of BLM data into the derivation of these predictors generally increases the correlation. For example, the correlation coefficient for WMX increases from 0.32 to 0.45.

The experimental thunderstorm probability equation shown in Table 3 was derived from forecasts and observations made on days from 15 March to 15 September, during 1980, 1981, and 1983. Data from 1982 were withheld to provide an independent sample for verification. The development sample consists of 321,998 cases (456 days times 714 grid blocks minus some cases with missing

observations). Thunderstorm frequency within the sample was 31%. The most highly correlated predictor, RN, reflects the presence of instability through a deep layer of the atmosphere and abundant low-level moisture (as does the K index). Apparently the BLM forecasts aid in better delineation of regions favorable to convection. Some of the remaining predictors (500-mb wind speed and boundary-layer moisture convergence) are more strongly associated with severe thunderstorms. The total reduction of variance of 35.6% is somewhat higher than that for the current operational equation.

7. SEVERE LOCAL STORM PROBABILITY EQUATIONS

An important part of the daily forecast guidance issued by the National Meteorological Center is the conditional probability of severe thunderstorms. Previous experience has shown that the best results in generating reliable forecast equations are obtained when the development samples are stratified according to time of year (spring, summer and cold season) because of the large seasonal variations in severe local storm frequency.

In developing a conditional probability equation for severe local storms, we restrict our consideration to those grid blocks in which a thunderstorm occurred during the forecast period.

Table 4 shows the linear correlation coefficients for the leading operational predictors and the experimental predictors. These coefficients were derived from a total of 320 sample days during the period 15 March to 15 June, 1980-1983. The 1000-mb height field is strongly correlated to severe storms because it delineates favorable regions of low surface pressure and warm air. This predictor forms the basis for a linearized predictor that explains the greatest reduction of variance in the current operational equation. The third operational predictor shown is the product of the 850 mb-500 mb equivalent potential temperature lapse rate, and the amount of low-level synoptic-scale lifting. This predictor is important in the warm sector of developing low pressure systems.

The linearized updraft speed predictor WMX provides a measure of the amount of kinetic energy that can be released by convective overturning. Strong updraft speeds are commonly associated with severe weather at the ground. As a result, this quantity is very highly correlated with severe weather in the development sample. It is interesting to note that the correlation is higher than that for the lifted index. WMX provides a measure of the maximum temperature excess at any level within the cloud, while the lifted index shows only the excess at the 500-mb level. The cloud depth H is also well-correlated with severe storms since deeper clouds are associated with stronger thunderstorms in the spring.

The lowering of the correlation coefficients by the introduction of BLM data is probably due to the increased amount of spatial variability inherent in the predictor fields. The MOS statistical procedure does not adequately assimilate predictor fields that possess a large amount of variability. Small errors in phase and amplitude can result in poor correlation to discrete severe storm events. We found, as did Charba (1979), that spatial smoothing increased the predictors' correlation to severe storms. Predictor fields from the LFM are "smoother", and the correlation higher. In our opinion, it appears that special procedures or techniques may be required to adequately handle higher resolution in forecast fields in future MOS development work.

The resulting probability equation for severe local storms is shown in Table 5. The probability equation was derived from forecasts during the period 15 March to 15 June during 1980, 1981, and 1983, a total of 240 sample days, with 39,566 cases. Severe storms occurred in 8.4% of these cases. In contrast to the general thunderstorm equation, which is dominated by the first predictor, several terms contribute significantly to the reduction of variance. Most of the predictors are clearly associated with large-scale systems; large-scale warm advection and lifting, and the location of the polar jet, all contribute to severe weather in the spring. The 7.7% reduction of variance is comparable to that of the current operational equations.

Severe local storms during the summer months are relatively rare; in our data sample they accounted for only 5.2% of all thunderstorm cases. In the absence of synoptic-scale systems to organize strong thunderstorms, mesoscale and local topographic effects become important. The correlation coefficients for most of the predictors (Table 6) are lower during the summer months. The coefficient for the LFM-derived WMX*, however, decreases only slightly.

The summer severe storm probability equation (Table 7) was derived from 201 days' data, with a total of 57,495 thunderstorm cases. Only a few terms contribute any significant reduction of variance. The predictors WMX and B represent the combined effects of moisture convergence and destabilization, whether such destabilization occurs through large-scale motions or solar heating. The 500-mb wind speed probably represents the contribution of transient upper-air disturbances that sometimes organize strong convection during the summer. The 6.7% reduction of variance is slightly larger than that for the operational equation.

8. VERIFICATION

We used the experimental equations described earlier to generate forecasts of 12-36 h thunderstorm and severe local storm probability for a total of 166 days during the period 15 March-14 September, 1982. We compared the verification scores for these forecasts to the scores achieved by the current operational forecasts for the same 714-block geographic region during the same period. This region coincides roughly with the model domain shown in Fig. 2, except that areas over the Gulf of Mexico and the Atlantic Ocean were excluded.

It is interesting to note that the experimental equations for both thunderstorms and severe local storms yield a much larger number of high probability forecasts than appear in the operational forecasts (see Fig. 25). For example, the experimental equations generated about twice as many severe storm conditional probabilities in the 20-45% range. The higher probabilities are due in part to the fact that thunderstorm frequency was higher in the development data sample for the experimental equations (30.6% compared to 26.6%). Likewise, the summer severe storm frequency was higher in the experimental development sample. In addition, the operational equations were developed for a slightly larger geographical area; the data sample included 761 grid blocks compared to our study's 714. The BLM domain does not include southwest Texas and northern New England, areas which are covered by the operational forecasts.

To evaluate the bias or reliability of the thunderstorm forecasts, we computed observed thunderstorm frequencies for each of ten individual forecast percentage probability categories with limits of 0.00-0.09, 0.10-0.19,..., 0.90-0.99. This frequency is the number of MDR grid blocks with thunderstorms divided by the total number of grid blocks in that forecast category. The verification sample included 106,368 forecasts during the 1982 warm season (166 days times 714 blocks minus some cases eliminated due to missing observations). A total of 34,153 cases had thunderstorms, or an average frequency of 32.1%. The average experimental forecast probability was 34.5%, or 36,679 cases expected to be accompanied by thunderstorms. The operational forecasts had an average probability of 30.2% during the same period.

Plots of thunderstorm probability versus thunderstorm frequency are shown in Fig. 26. The data points are located at the average probability for each of the ten categories. The solid diagonal line represents perfect reliability. The experimental forecasts tend to overpredict thunderstorm frequency at probabilities below 50% and above 80%. Still, the bias is comparable to that of the operational forecasts, despite the greater number of large probabilities in the experimental forecasts.

To demonstrate the usefulness of the thunderstorm forecasts to the forecaster, we reduced the probability forecasts to categorical (yes-no) forecasts by applying a threshold value. The contingency table used in computing the verification scores for such forecasts is shown in Table 8. We define "x" as a "yes" forecast that verifies and "w" as a "no" forecast that verifies. The term "z" represents a "false alarm", and "y" a missed event. The probability of detection (POD) is given by $x/(x+y)$, the false alarm ratio (FAR) by $z/(x+z)$, and the critical success index (CSI) by $x/(x+y+z)$. The forecast bias, or the ratio of number of events expected to the number observed, is given by $(x+z)/(x+y)$. The scores are defined in detail by Donaldson et al. (1975).

The expected accuracy of the categorical forecasts as a function of probability threshold is shown in Figs. 27 and 28. We see that the CSI or "threat score" for the experimental forecasts is higher than that for the operational forecasts at most threshold values. The POD and bias in the experimental forecasts are higher, possibly because of the greater number of high probability forecasts.

The bias or reliability of the 12-36 h conditional severe local storm probability forecasts during the spring season (15 March-15 June) is shown in Tables 9 and 10. The experimental forecasts were very accurate up to about 24% probability. The observed frequency of severe storms was about 10.2%, while the average probability of the experimental forecasts was 8.9%, compared to 6.5% for the operational forecasts.

The experimental severe storm forecasts were significantly more reliable than the operational ones during the summer season (16 June-14 September). Both the average forecast probability and the mean probabilities in many of the individual categories (Tables 11 and 12) were closer to the observed frequencies. Again, this might be due in part to the nature of the data samples used to generate the two sets of forecasts equations. The relative frequency of severe storms in the experimental data sample (5.5%) was closer to the observed relative frequency during 1982 (5.0%) than was the relative frequency in the sample used to develop the operational equations (3.4%).

Forecasts of unconditional severe storm probability are useful in determining areas that are at particular risk of violent weather, and in preparing automated convective outlook forecasts. In practice, we compute these forecasts by multiplying the conditional severe storm probability by the thunderstorm probability. The bias of these forecasts is shown in Tables 13 and 14. Over the entire warm season, the forecasts derived from the experimental equations were very reliable up to about 24%, even though the event frequency was only 2.2%. The operational forecasts tended to underpredict the frequency in the lower probability categories, where most of the forecasts occur. The average experimental forecast probability was 2.3%, compared to 1.4% for the operational forecasts.

Again, we computed yes-no forecasts for severe local storm occurrence by selecting a threshold for the unconditional probabilities. The verification scores for the period 15 March-15 June are shown in Fig. 29. The POD and CSI for the experimental forecasts are higher at most probability thresholds, though the FAR and bias (not shown) are higher, as well. At the threshold yielding any given POD, the experimental forecasts generally have a lower bias and FAR. For example, at a POD of 0.45, the experimental forecasts have a FAR of 0.83 and a bias of 2.7, while the operational forecasts have a FAR of 0.86 and a bias of 3.6.

We found similar characteristics in the scores for the categorical severe local storm forecasts during the summer period (16 June-14 September). The skill in both sets of forecasts decreases during this period, as shown in Fig. 30. This decrease reflects the lower frequency of severe storms and the predominance of sub-synoptic effects in causing them.

9. SUMMARY AND CONCLUSIONS

We have derived a set of new predictors based on cumulus dynamics for possible use in MOS forecasts of 12-36 h thunderstorm and severe local storm probability. The predictors were designed to use temperature, moisture, and pressure profiles from the National Meteorological Center's LFM model and the Techniques Development Laboratory's BLM. One of the main goals of the study was to assess the impact of the BLM's finer vertical and horizontal computational mesh on the accuracy of MOS probability forecasts.

The experimental predictors were derived from an entraining jet model of cumulus clouds and from a stability analysis using the parcel method. A preliminary investigation showed that these quantities reflected observed convective activity in a reasonable manner. Certain cumulus cloud properties (rainout and maximum updraft speed) proved to be highly correlated to general thunderstorm and severe thunderstorm activity, respectively. The introduction of BLM forecast data increased the predictors' correlation with general thunderstorm activity but tended to lower the predictors' correlation with severe thunderstorm occurrence. The latter result is likely due to the inability of the current linear screening regression procedure to handle the increased amount of spatial details in the predictor fields.

We derived new probability forecast equations that included the experimental predictors along with the operational predictors. A verification study on one season of independent data showed that the new equations gave some

improvement over the current operational equations. The bias in the new probability forecasts was no larger than that in the operational forecasts. The critical success index for categorical forecasts from the new equations was higher.

In future work, we plan to test new predictors as they become available. Since the current linear regression techniques do not make the best possible use of the highly detailed forecasts from the BLM, we have begun examining BLM forecast fields for characteristic spatial patterns in the vicinity of observed severe storms.

ACKNOWLEDGMENTS

I could not have carried out this study without the help of many people, who aided me in computer programming and interpreting some of the initial results. In particular, I wish to thank Ms. Melvina McDonald, who assisted me in obtaining MDR data and severe storm reports; Ms. Janice Washington and Mrs. Belinda Howard, who typed drafts of this report; Mr. Henry Robinson, who provided the original code for the cloud model used in these experiments; Mr. Ronald Reap, who gave general guidance as to the course of the work; and Dr. Wilson Shaffer, who provided important information about TDL's boundary-layer model.

REFERENCES

Charba, J., 1979: Two-six hour severe local storm probabilities: An operational forecasting system. Mon. Wea. Rev., 107, 268-282.

Crum, T., and J. Cahir, 1983: Experiments in shower-top forecasting using an interactive one-dimensional cloud model. Mon. Wea. Rev., 111, 829-835.

Donaldson, R., Jr., R. Dyer, and M. Kraus, 1975: An objective evaluator of techniques for predicting severe weather events. Preprints Ninth Conference Severe Local Storms, Norman, Amer. Meteor. Soc., 321-326.

Fields, R. I., and H. W. Robinson, 1971: Modeling trade cumuli and salt seeding. Report No. 18 to the National Science Foundation, NSF GA 13818, The Pennsylvania State University, 147 pp.

Foster, D., and R. M. Reap, 1978: Archiving the new manually digitized radar data. TDL Office Note 78-5, National Weather Service, NOAA, U.S. Department of Commerce, 15 pp.

Gerrity, J. F., 1977: The LFM model - 1976: A documentation. NOAA Technical Memorandum. NWS NMC-60, National Oceanic and Atmospheric Administration, U.S. Department of Commerce, 68 pp. [NTIS P13 279 419/6].

Glahn, H. R., and D. A. Lowry, 1972. The use of Model Output Statistics (MOS) in objective weather forecasting. J. Appl. Meteor., 11, 1203-1211.

Hess, S., 1959: Introduction to theoretical meterology. New York, Holt and Company, 362 pp.

Kessler, E., 1969: On the distribution and continuity of water substance in in atmospheric circulation. Meteorological Monographs, Vol. 10, Amer. Meteor. Soc., Boston, 84 pp.

Kreitzberg, C., M. Leach and R. Rasmussen, 1978: Convective precipitation prediction tests using a cumulus model. Final Contract Report 5-35361, Techniques Development Laboratory, National Weather Service, U.S. Department of Commerce, Silver Spring, Md., 37 pp.

Long, P. E., W. A. Shaffer, J. E. Kemper and F. J. Hicks, 1978: The state of the Techniques Development Laboratory's boundary-layer model: May 24, 1977. NOAA Technical Memorandum NWS TDL-66, National Oceanic and Atmospheric Administration, U.S. Department of Commerce, 58 pp. [NTIS PB 287 821/3].

Miller, R. C., 1972: Notes on analysis and severe storm forecasting procedures of the Air Force Global Weather Center. Air Weather Service Tech. Rep. 200 (Rev.), U.S. Air Force, 102 pp. [NTIS AD 744 042].

NOAA; 1983: Storm Data. ISSN 0039-1972, National Climatic Date Center, National Oceanic and Atmospheric Administration, U.S. Department of Commerce.

Reap, R. M., 1972: An operational three-dimensional trajectory model. J. Appl. Meteor., 11, 1193-1202.

____, and D. S. Foster, 1979: Automated 12-36 hour probability forecasts of thunderstorms and severe local storms. J. Appl. Meteor., 18, 1304-1315.

Sanders, F., and A. Garrett, 1975: Application of a convective plume model to prediction of thunderstorms. Mon. Wea. Rev., 103, 874-877.

Shaffer, W., J. Kemper, and P. Long, 1979: Potential thunderstorm forecast guidance products from the Techniques Development Laboratory's boundary layer model. Preprints Eleventh Conference on Severe Local Storms, Kansas City, Amer. Meteor. Soc., 151-157.

Simpson, J., and V. Wiggert, 1969: Models of precipitating cumulus towers. Mon. Wea. Rev., 97, 471-489.

Stone, H. M., 1983: Stability analysis program, NOAA Eastern Region Computer Programs and Problems NWS ERCP-No. 9., National Weather Service, NOAA, U.S. Department of Commerce, 28 pp.

Weinstein, A., and L. Davis, 1968: A parametrized numerical model of cumulus convection. Report No. 11 to the National Science Foundation, NSF GA-777, The Pennsylvania State University, 44 pp.

APPENDIX

Entraining Jet Cumulus Model

The entraining jet cloud model is based on an equation which yields the cloud updraft speed as a function of height. This equation for vertical motion (w) is

$$\frac{d(w^2)}{dz} = \frac{2g}{T_{ve}} (T_{vc} - T_{ve}) - 2 g q_l - \mu w^2 \qquad \text{(A1)}$$

where g is the gravitational acceleration;
T_{ve} is the environmental virtual temperature;
T_{vc} is the incloud virtual temperature; and
q_l is the liquid water mixing ratio.

The entrainment factor μ is an empirical function of the updraft R and is given by

$$\mu = 0.2/R$$

Thus, the first term on the right side represents buoyancy, the second liquid water drag, and the third the slowing effects of lateral entrainment. Some cloud models include a "virtual mass" term to represent the influence of an incloud pressure perturbation. Because we are concerned only with the long-term statistical relationship between some cloud properties and thunderstorm occurrence, we neglected this term.

The incloud temperature (T_c) and moisture profiles are determined from the differential equation of pseudoadiabatic ascent modified by entrainment (Hess, 1959):

$$-\frac{dT_c}{dz} = \frac{\frac{g}{C_p}\left[1 + \frac{L}{R_d}\frac{q_c}{T}\right] + \left(\frac{1}{m}\right)\left(\frac{dm}{dz}\right)\left[(T_c - T_e) + \frac{L}{c_p}(q_c - q_e)\right]}{1 + \frac{L^2 \varepsilon q_s}{C_p R_d T^2}} \qquad \text{(A2)}$$

where $\varepsilon = 0.622$;
R_d is the gas constant for dry air;
C_p is the specific heat of air at constant pressure;
T_c and T_e are incloud and environment temperature, respectively;
q_c and q_e are incloud and environment mixing ratio;
L is the latent heat of condensation; and
$(1/m)\ (dm/dz)$ is the entrainment rate, earlier given as μ.

In order to compute the rain production by the cloud, we incorporate three equations for the formation and fallout of rainwater. All condensing water is assumed to form cloud droplets, initially. The following empirical relationship gives the amount of rainwater produced from cloudwater by "autoconversion":

$$dQ_{cl} = a\,(Q_{cl} - 0.5)\;dt \quad \text{for } Q_{cl} > 0.5 \qquad \text{(A3)}$$
$$= 0 \qquad \text{for } Q_{cl} = 0.5$$

where Q_{cl} is cloudwater mixing ratio in g m^{-3} and dQ_{cl} is the amount of rainwater formed in the time interval dt. The constant a = .001 was suggested by Kessler (1969).

Another empirical relationship accounts for the collection of cloud droplets by raindrops falling through cloudy air:

$$dQ_{coll} = b\,Q_{cl}\,dt\,(Q_r^{.875}) \quad \text{for } Q_r > 0 = 0 \text{ otherwise} \qquad \text{(A4)}$$

where dQ_{coll} is the amount of rainwater formed by cloud drop collection, Q_r is the rainwater mixing ratio in g m^{-3} and b is set to 0.00526 after Kessler (1969).

Finally, a third relationship provides an estimate of the rate at which rainwater falls from a given region of the cloud. This fallout is a function of the rainwater concentration and the updraft speed and is given by

$$dQ_{fall} = Q_{rg}\;[BK + BK^2/2 + BK^3/6]e^{-BK} \qquad \text{(A5)}$$

where

$$BK = [w^2 \times 2.5 \times 10^6]\;Q_{rg}^{-.25}$$

and Q_{rg} is the gravimetric rainwater mixing ratio (g g^{-1}). This formulation has been referred to as the "Lopez water wheel" (Fields and Robinson, 1968).

To find the profiles of vertical velocity and temperature, we first select a cloud base height (in practice, the cloud condensation level of the given sounding), then prescribe cloud base values of w, q, and T. In this study, we set w=1 m s^{-1} and set T to the environmental temperature. We assume that the incloud air is saturated and that the liquid water mixing ratio is zero at cloud base. Using these initial values for w and T, (A1) and (A2) are integrated with respect to z by the Euler method with a step length of 100 m. At the end of each step, the amount of newly condensed cloud water is computed from the difference in saturation mixing ratio between the top and bottom of the 100-m layer. The changes in Q_{cl} and Q_r are then computed from (A3)-(A5) and the total rainfall stored for later use as a thunderstorm predictor. We take the cloud top to be the level at which the updraft speed vanishes.

Table 1. List of experimental and operational predictors employed in the screening regression procedure

Experimental predictors
Cumulus cloud depth (H)
Maximum cumulus updraft speed (WMX)
Cumulus cloud rainout (RN)
Convective available potential energy term (B)
Product of B and boundary-layer moisture convergence (MB)
Best lifted index (BLI)
K index from BLM and LFM input
Operational predictors, thunderstorm equation
K index
Product of K index and local climatological frequency (KF_{lin})
500-mb wind speed
Boundary-layer moisture convergence
Surface dewpoint
1000-400 mb mean relative humdity
Surface-700 mb mean relative humidity
Operational predictors, severe local storm equation, spring
1000-mb height
Total totals index
850-mb temperature advection
Solar altitude
850-500 mb temperature lapse rate
1000-400 mb mean relative humidity
Surface convergence
Convective instability times 700 mb 12-h net vertical displacement (CINVD)
Operational predictors, severe local storm equation, summer
1000-mb height
500-mb wind speed
Surface temperature
Total totals index

Table 2. Linear correlation of thunderstorm predictors with thunderstorm activity observed by radar for period 15 March to 15 September for years 1980-83. All predictors are 24-h forecasts based on 0000 GMT initial data. Asterisk (*) indicates linearized predictor, single prime (') indicates predictor smoothed by 5-point averaging, double prime ('') indicates predictor smoothed by 9-point averaging. Predictor definitions: RN = rainout; H = cloud depth; WMX = maximum cumulus updraft speed; B = convective available potential energy; MB = B x moisture convergence; KF* = linearized product of K index and climatological thunderstorm frequency

Predictor	Model	Correlation
	(Leading operational predictors)	
K index*	LFM/Trajectory	0.49
KF*	LFM	0.46
Surface dewpoint	Trajectory	0.39
	(Experimental predictors)	
K index''	BLM/LFM	0.43
RN''	LFM	0.32
H''	LFM	0.44
WMX''	LFM	0.32
B''	LFM	0.32
RN''	BLM/LFM	0.43
H''	BLM/LFM	0.48
WMX''	BLM/LFM	0.45
B''	BLM/LFM	0.37
MB''	BLM/LFM	0.30
RN*''	LFM	0.44
RN*''	BLM/LFM	0.51
MB*''	BLM/LFM	0.37
BLI*''	BLM/LFM	-0.44
K index*''	BLM/LFM	0.48

Table 3. Thunderstorm probability equation for period 15 March to 15 September. Predictor abbreviations explained in Table 2.

Predictor	Model	Coefficient	Reduction of Variance (%)
Constant	--	-27.37	--
RN*''	BLM/LFM	0.4793	--
K index*	LFM/Trajectory	0.6848	4.86
Boundary layer moisture divergence	LFM	-.2813	1.15
KF*''	LFM	0.01745	0.87
500-mb wind speed'	LFM	0.8198	1.76
RN*	LFM	0.4893	0.35
B*''	LFM	-0.06998	0.54
Mean relative humidity	LFM	0.2166	0.34
		TOTAL	35.64

Table 4. Linear correlation of predictors with severe thunderstorm activity for period 15 March to 15 June for years 1980-83. All predictors are 24-h forecasts based on 0000 GMT initial data. Predictor definitions as in Table 1.; CINVD = product of convective instability an low-level vertical displacement.

Predictor	Model	Correlation
	(Leading operational predictors)	
1000-mb height	LFM	-0.19
Total totals index*	LFM/Trajectory	0.18
CINVD*	Trajectory	0.17
	(Experimental predictors)	
RN''	LFM	0.18
H''	LFM	0.17
WMX''	LFM	0.18
B''	LFM	0.15
RN''	BLM/LFM	0.15
H''	BLM/LFM	0.11
WMX''	BLM/LFM	0.07
B''	BLM/LFM	0.14
MB''	BLM/LFM	0.14
H*''	LFM	0.18
H*''	BLM/LFM	0.12
B*''	LFM	0.15
B*''	BLM/LFM	0.14
WMX*''	LFM	0.19
WMX*''	BLM/LFM	0.12
BLI*''	BLM/LFM	-0.08

Table 5. Severe local storm probability equation for period 15 March to 15 June. Predictor abbreviations explained in Table 2; T50T85 = 500-mb temperature minus 850-mb temperature.

Predictor	Model	Coefficient	Reduction of Variance (%)
Constant	--	-42.65	--
WMX*''	LFM	0.2722	3.55
500-mb wind speed'	LFM	0.4225	1.81
MB*''	BLM/LFM	0.1610	0.95
Total totals index	LFM/Trajectory	0.2996	0.62
CINVD*	Trajectory	0.2555	0.22
T50T85'	LFM	-0.4383	0.20
H*''	BLM/LFM	0.6073	0.17
1000-mb height	LFM	-0.02454	0.18
		TOTAL	7.70

Table 6. As in Table 4., except for period 16 June to 15 September for years 1980-82, and 16 June to 16 August, 1983.

Predictor	Model	Correlation
	(Leading operational predictors)	
1000-mb height	LFM	-0.17
Total totals index*	LFM/Trajectory	0.16
	(Experimental predictors)	
RN''	LFM	0.13
H''	LFM	0.14
WMX''	LFM	0.17
B	LFM	0.13
RN''	BLM/LFM	0.08
H''	BLM/LFM	0.05
WMX''	BLM/LFM	0.03
B''	BLM/LFM	0.11
MB	BLM/LFM	0.05
H*''	LFM	0.15
H*''	BLM/LFM	0.13
WMX*''	LFM	0.19
WMX*''	BLM/LFM	0.03
B*''	LFM	0.15
B*''	BLM/LFM	0.15

Table 7. Severe thunderstorm probability equation for period 16 June to 15 September. Predictor definitions explained in Table 1.

Predictor	Model	Coefficient	Reduction of Variance (%)
Constant	--	-25.40	--
WMX*''	LFM	0.2520	2.86
500 mb wind speed	LFM	0.8260	2.83
B''	BLM/LFM	0.01478	0.69
B	LFM	0.01098	0.16
Total totals index*	LFM/Trajectory	0.3340	0.11
			TOTAL 6.66

Table 8. Contingency table used in computing scores for categorical forecasts.

Observed	Predicted		
	Thunder-storm	No Thunder-storm	Total
Thunderstorm	x	y	x+y
No thunderstorm	z	w	z+w
Total	x+z	y+w	x+y+z+w

Table 9. Bias or reliability of the experimental 12-36 h severe local storm conditional probability forecasts for the period 15 March-15 June, 1982.

Probability category	Number of thunderstorm cases	Expected number of severe cases*	Observed number of severe cases	Average forecast probability	Observed probability of occurrence
0.40-0.44	10	4	7	0.41	0.70
0.35-0.39	71	26	32	0.37	0.45
0.30-0.34	221	71	84	0.32	0.38
0.25-0.29	423	115	155	0.27	0.37
0.20-0.24	694	153	186	0.22	0.27
0.15-0.19	1365	234	249	0.17	0.18
0.10-0.14	2435	299	312	0.12	0.13
0.05-0.09	3588	265	267	0.07	0.07
0.0 -0.04	5347	93	151	0.02	0.03
Total	14154	1260	1443	0.09	0.10

*The expected number of severe cases is computed by multiplying the average probability for each category by the number of thunderstorm cases.

Table 10. As in Table 9, except for operational forecasts.

Probability category	Number of thunderstorm cases	Expected number of severe cases	Observed number of severe cases	Average forecast probability	Observed probability of occurrence
0.40-0.44	4	1	2	0.41	0.50
0.35-0.39	30	11	11	0.37	0.37
0.30-0.34	95	30	38	0.32	0.40
0.25-0.29	210	57	58	0.27	0.28
0.20-0.24	379	83	85	0.22	0.22
0.15-0.19	919	156	217	0.17	0.24
0.10-0.14	1837	224	357	0.12	0.19
0.05-0.09	3270	234	366	0.07	0.11
0.0 -0.04	7410	120	309	0.02	0.04
Total	14154	916	1443	0.06	0.10

Table 11. As in Table 9, except for experimental 12-36 h forecasts during the period 16 June-14 September, 1982.

Probability category	Number of thunderstorm cases	Expected number of severe cases	Observed number of severe cases	Average forecast probability	Observed probability of occurrence
0.40-0.44	0				
0.35-0.39	0				
0.30-0.34	0				
0.25-0.29	13	3	13	0.26	1.00
0.20-0.24	128	27	38	0.21	0.30
0.15-0.19	764	128	141	0.17	0.18
0.10-0.14	2637	321	327	0.12	0.12
0.05-0.09	5796	414	306	0.07	0.05
0.0 -0.04	11137	226	192	0.02	0.02
Total	20474	1119	1017	0.05	0.05

Table 12. As in Table 11, except for operational forecasts.

Probability category	Number of thunderstorm cases	Expected number of severe cases	Observed number of severe cases	Average forecast probability	Observed probability of occurrence
0.40-0.44	0				
0.35-0.39	3	1	3	0.37	1.00
0.30-0.34	7	2	7	0.32	1.00
0.25-0.29	7	1	7	0.26	1.00
0.20-0.24	30	6	22	0.22	0.73
0.15-0.19	62	10	23	0.17	0.37
0.10-0.14	548	63	86	0.12	0.16
0.05-0.09	4393	294	412	0.07	0.09
0.0 -0.04	15424	324	457	0.02	0.03
Total	20474	701	1017	0.03	0.05

Table 13. Bias or reliability of the experimental 12-36 h unconditional severe storm probability forecasts during the period 15 March-14 September, 1982.

Probability category	Number of thunderstorm cases	Expected number of severe cases*	Observed number of severe cases	Average forecast probability	Observed probability of occurrence
0.40-0.44	0	0	0	0	0
0.35-0.39	6	2	2	0.36	0.33
0.30-0.34	56	17	37	0.31	0.66
0.25-0.29	177	48	72	0.27	0.41
0.20-0.24	439	97	113	0.22	0.26
0.15-0.19	959	164	187	0.17	0.19
0.10-0.14	3184	380	373	0.12	0.12
0.05-0.09	12488	866	744	0.07	0.06
0.0 -0.04	101215	1126	932	0.01	0.01
Total	118524	2700	2460	0.02	0.02

*The expected number of severe cases in computed by multiplying the average probability for each category by the number of cases.

Table 14. As in Table 13, except for operational forecasts.

Probability category	Number of thunderstorm cases	Expected number of severe cases	Observed number of severe cases	Average forecast probability	Observed probability of occurrence
0.40-0.44	0	0	0	0	0
0.35-0.39	0	0	0	0	0
0.30-0.34	7	2	4	0.32	0.57
0.25-0.29	19	5	6	0.27	0.32
0.20-0.24	61	13	26	0.22	0.43
0.15-0.19	284	47	67	0.17	0.24
0.10-0.14	1207	143	213	0.12	0.18
0.05-0.09	5775	390	564	0.07	0.10
0.0 -0.04	111171	1092	1580	0.01	0.01
Total	118524	1692	2460	0.01	0.02

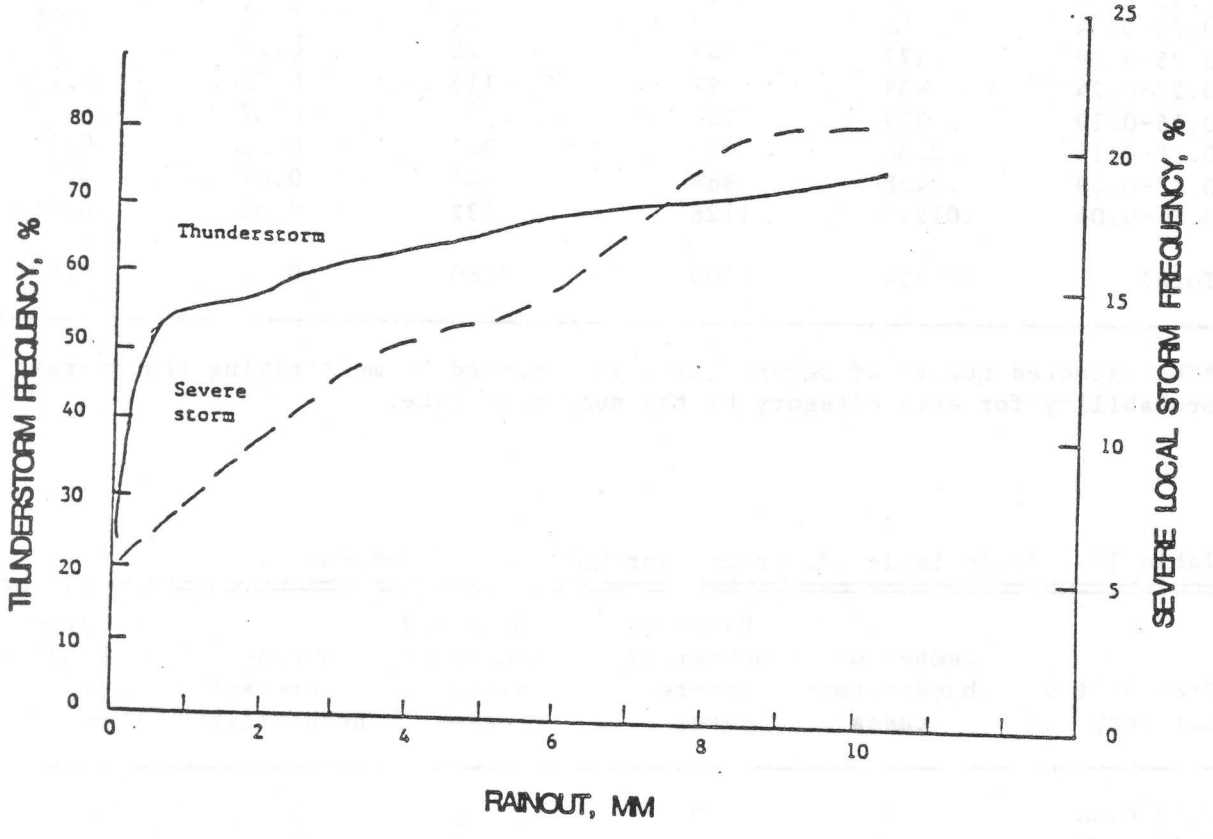

Figure 1. Forecast rainout (RN) vs. observed thunderstorm and severe local storm frequency.

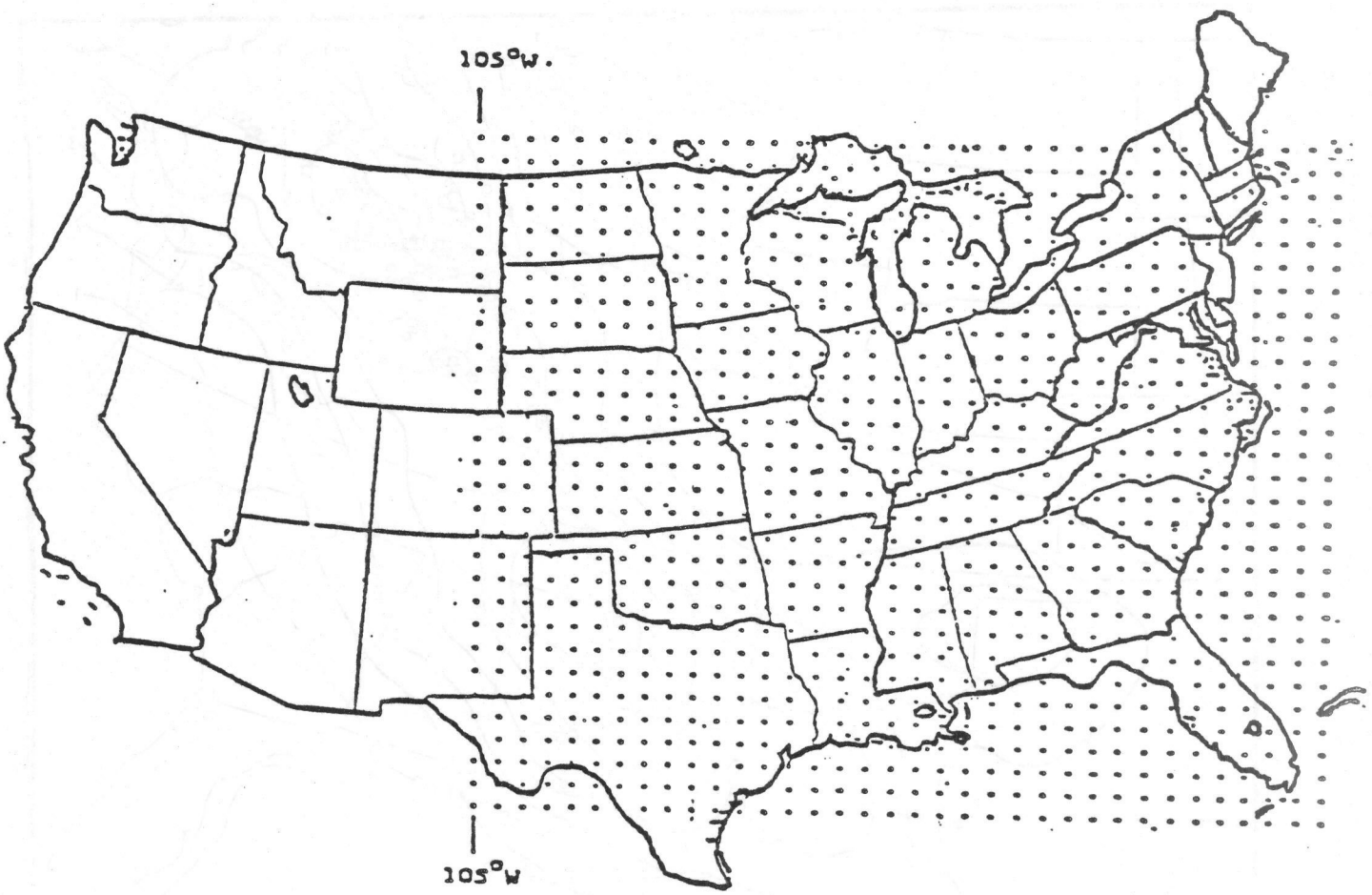

Figure 2. Domain of the Techniques Development Laboratory's boundary-layer model.

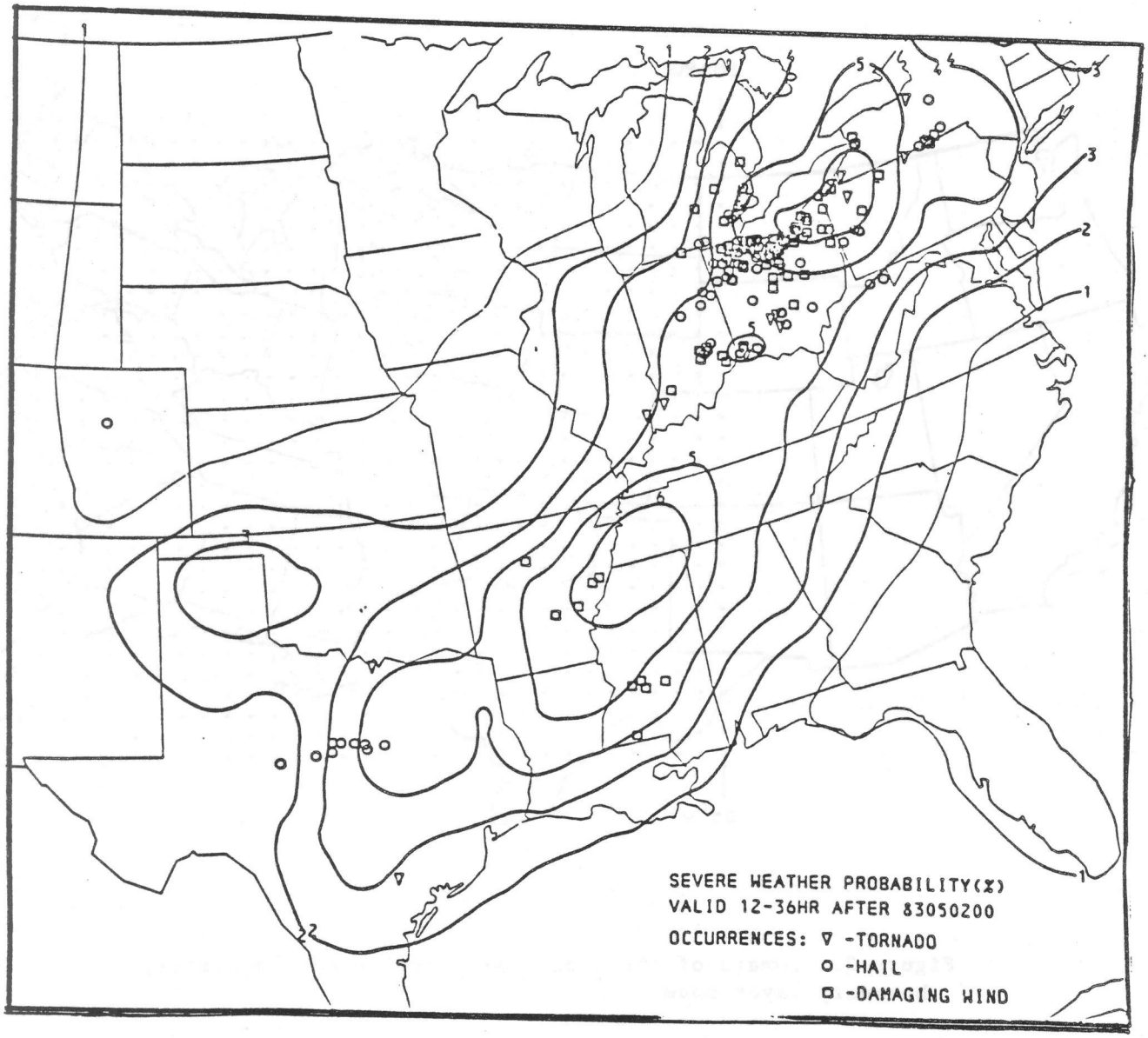

Figure 3. MOS unconditional severe storm probability and severe storm reports during the period 12-36 h after 0000 GMT, 2 May 1983.

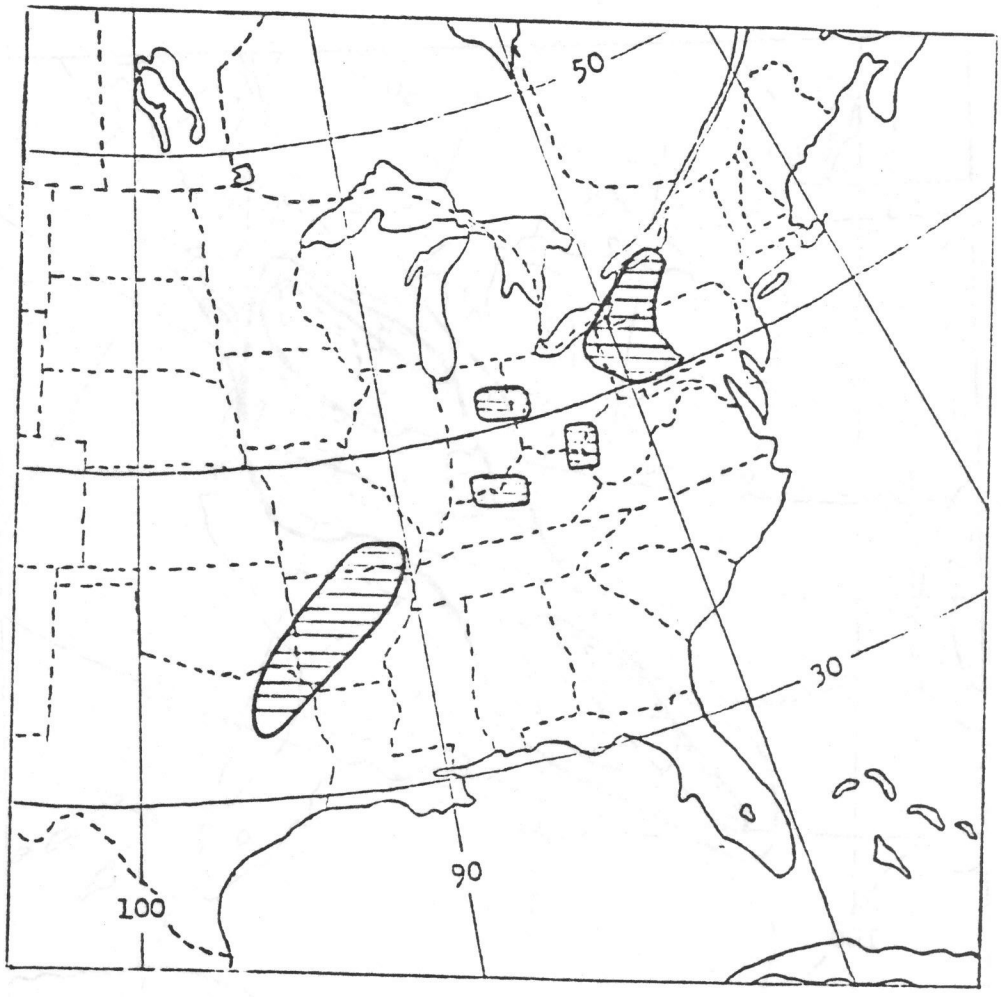

Figure 4. Areas with radar echoes of VIP3 level intensity or greater at 0000 GMT, 3 May 1983.

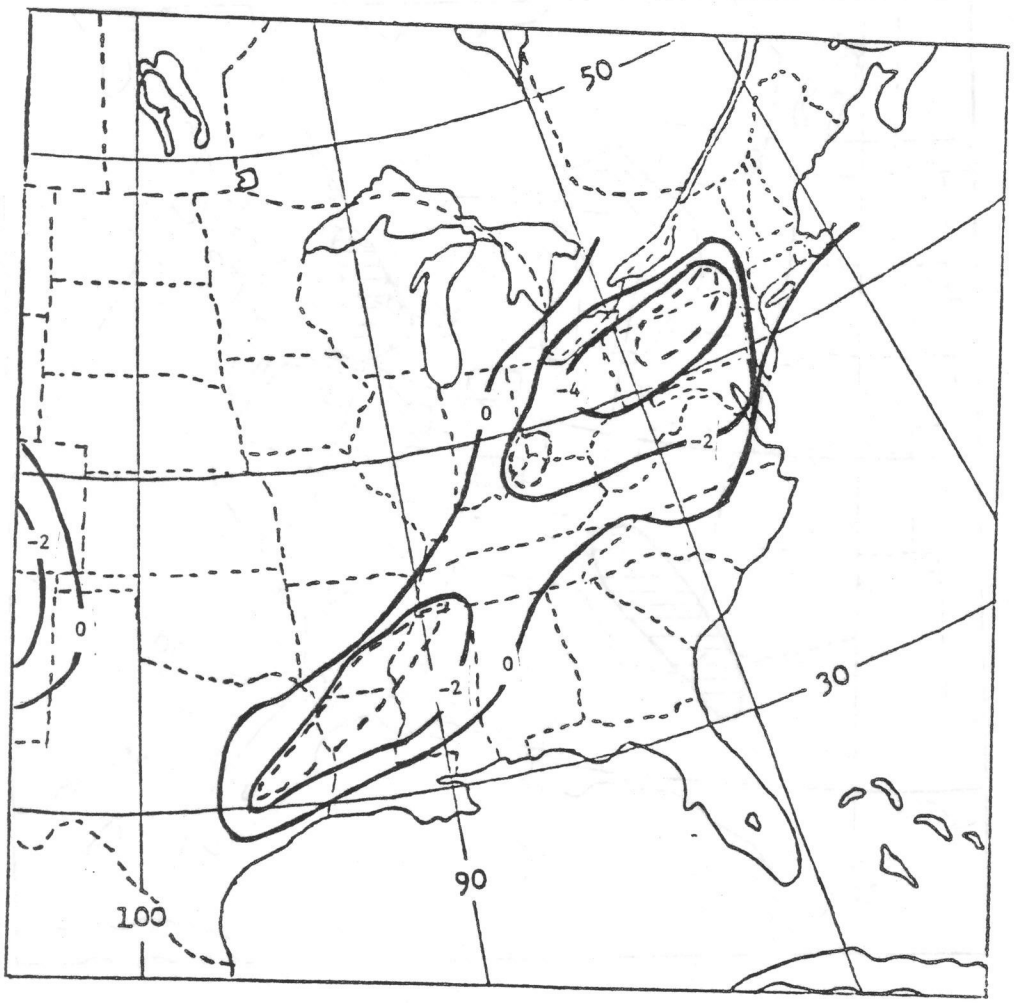

Figure 5. Best lifted index (BLI), K, 24-h forecast valid 0000 GMT, 3 May 1983. Dashed lines enclose areas in which moisture convergence is greater than 1 g kg^{-1} h^{-1}.

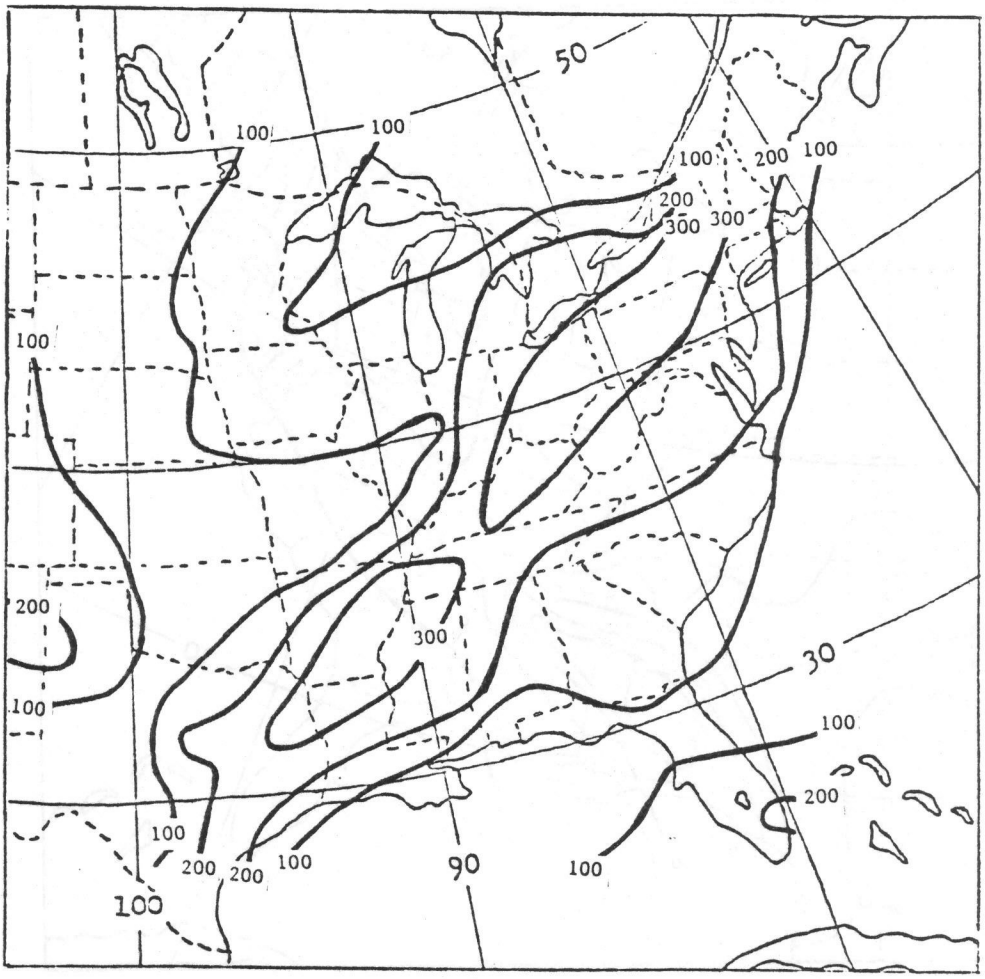

Figure 6. BLM cloud depth (H), mb, 24-h forecast valid 0000 GMT, 3 May 1983.

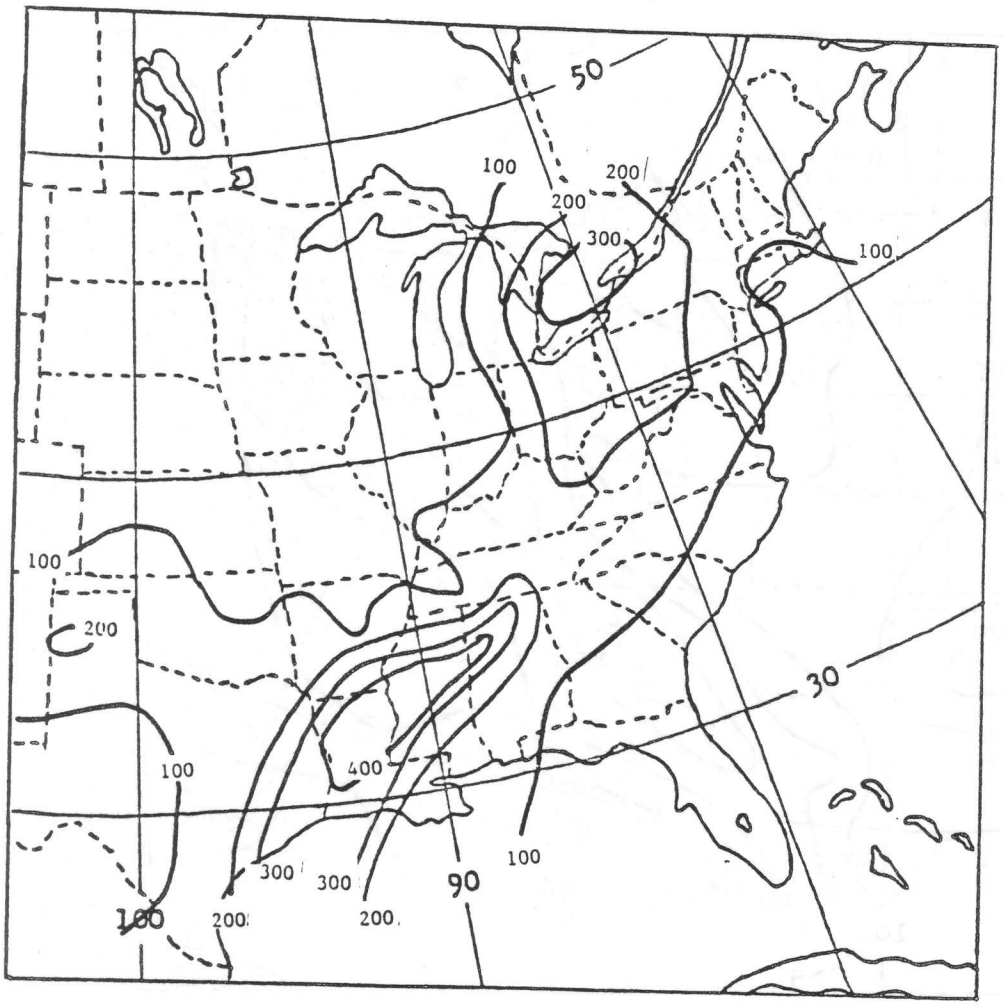

Figure 7. LFM cloud depth (H), mb, 24-h forecast valid 0000 GMT, 3 May 1983.

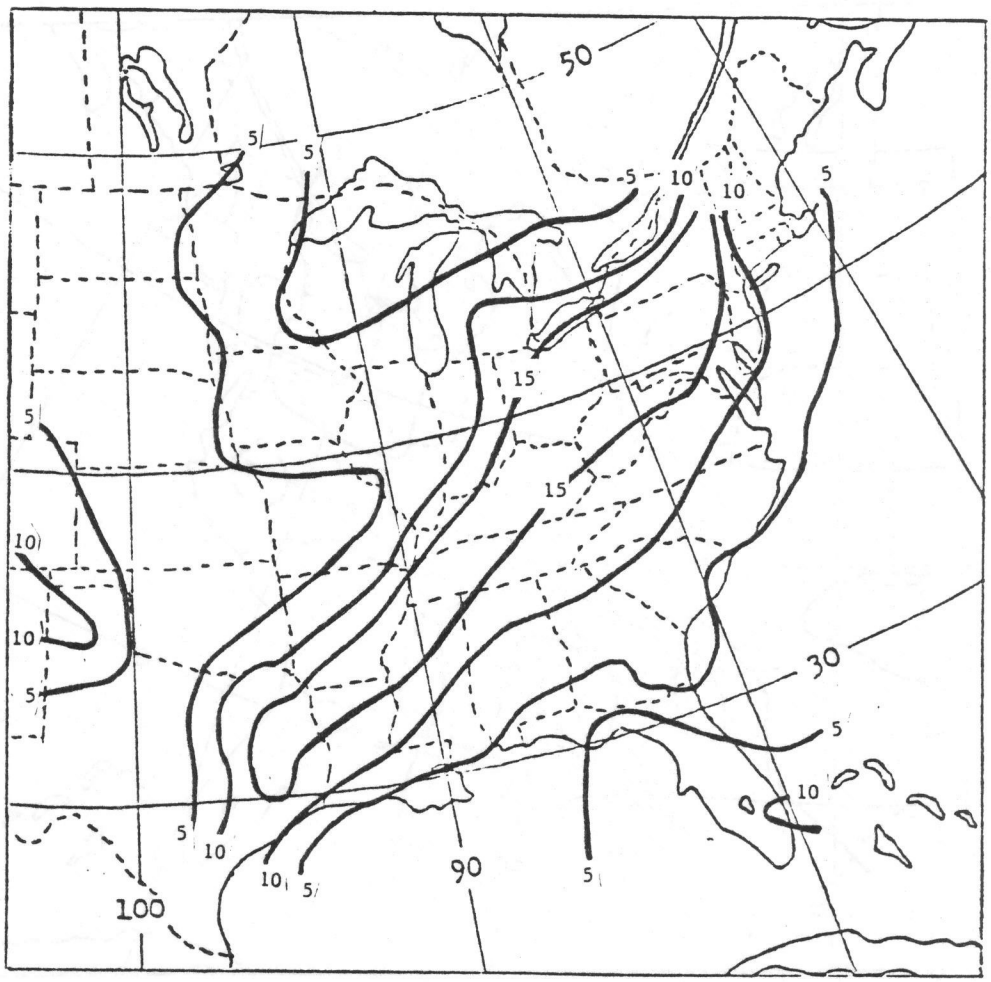

Figure 8. BLM cumulus updraft speed (WMX), m s^{-1}, 24-h forecast valid 0000 GMT, 3 May 1983.

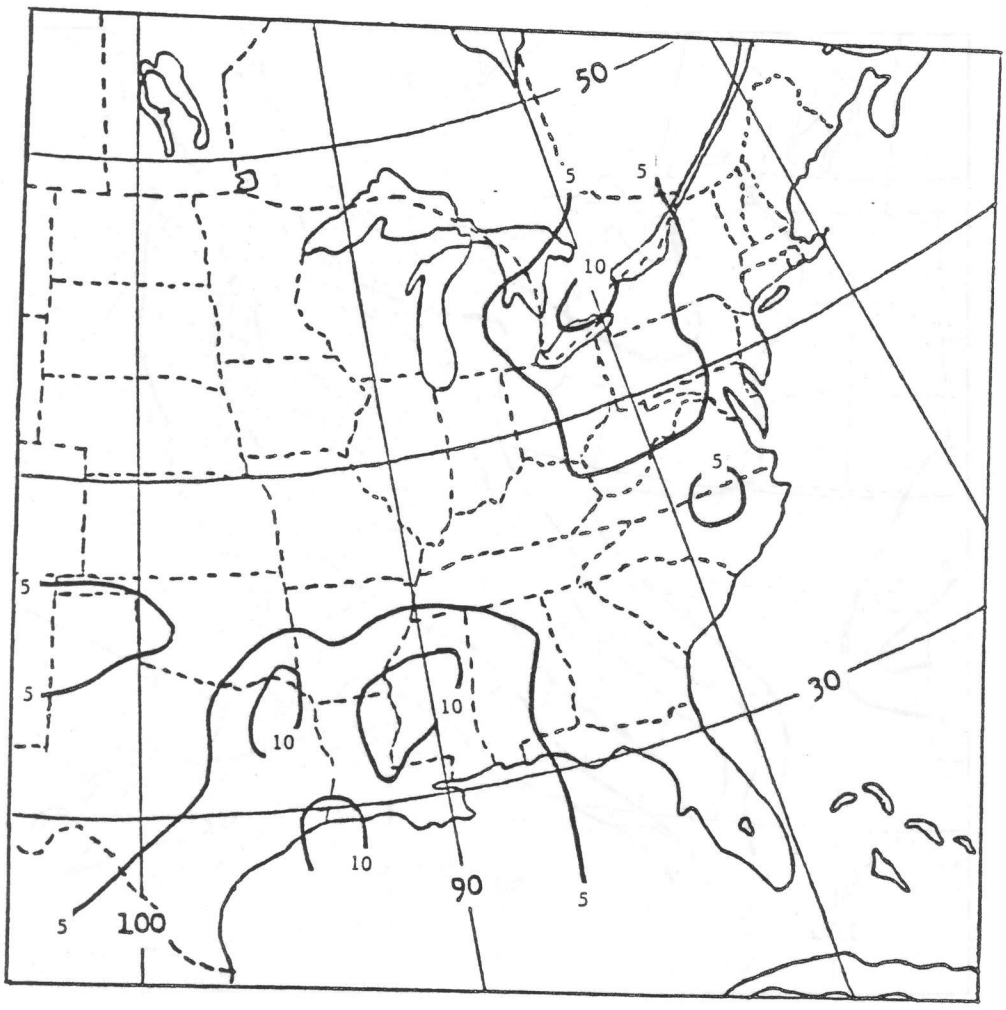

Figure 9. LFM cumulus updraft speed (WMX), m s^{-1}, 24-h forecast valid 0000 GMT, 3 May 1983.

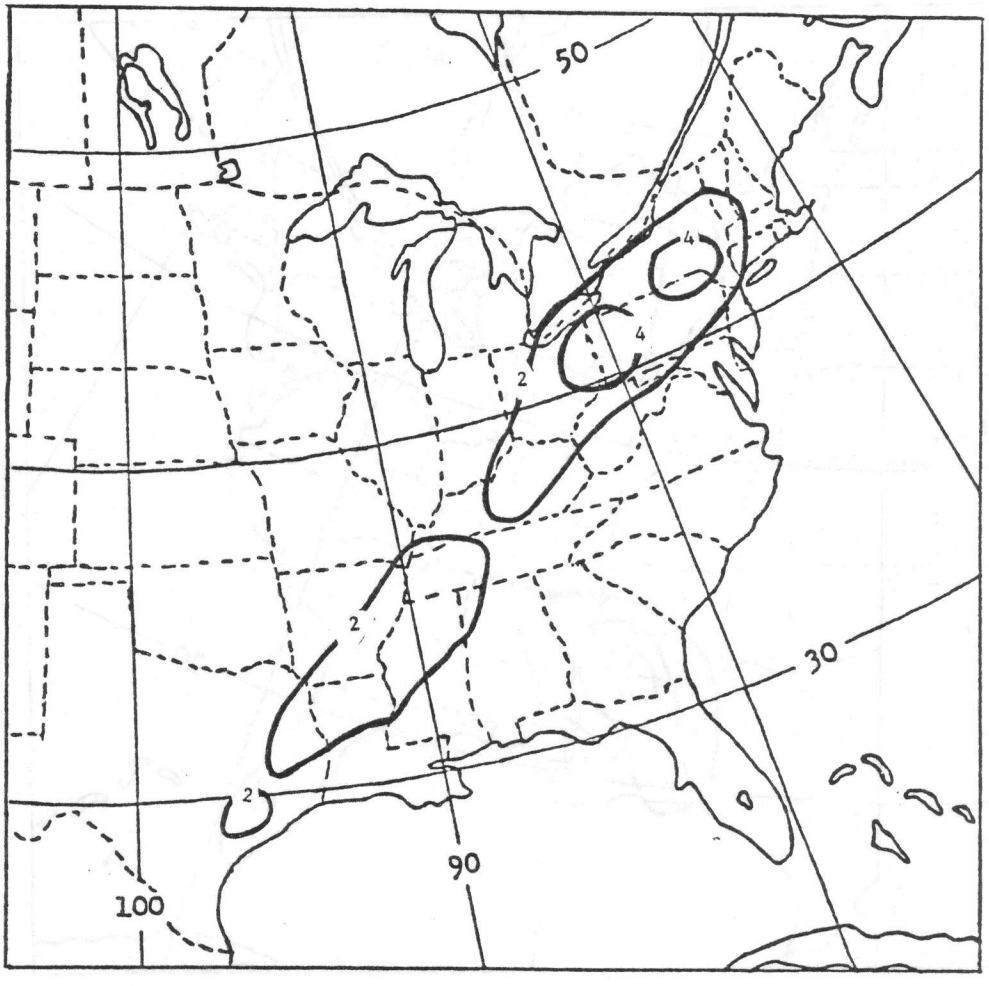

Figure 10. BLM rainout term (RN), mm water, 24-h forecast valid 0000 GMT, 3 May 1983.

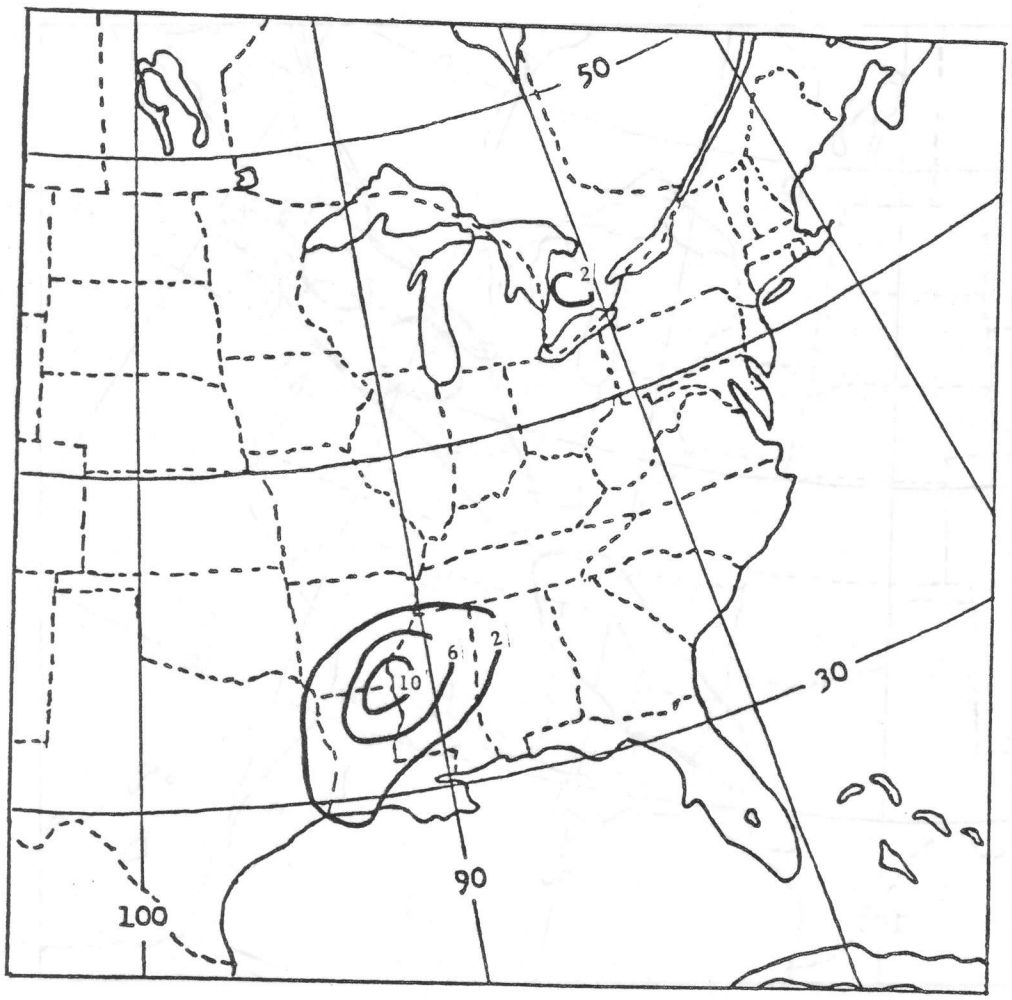

Figure 11. LFM rainout term (RN), mm water, 24-h forecast valid 0000 GMT, 3 May 1983.

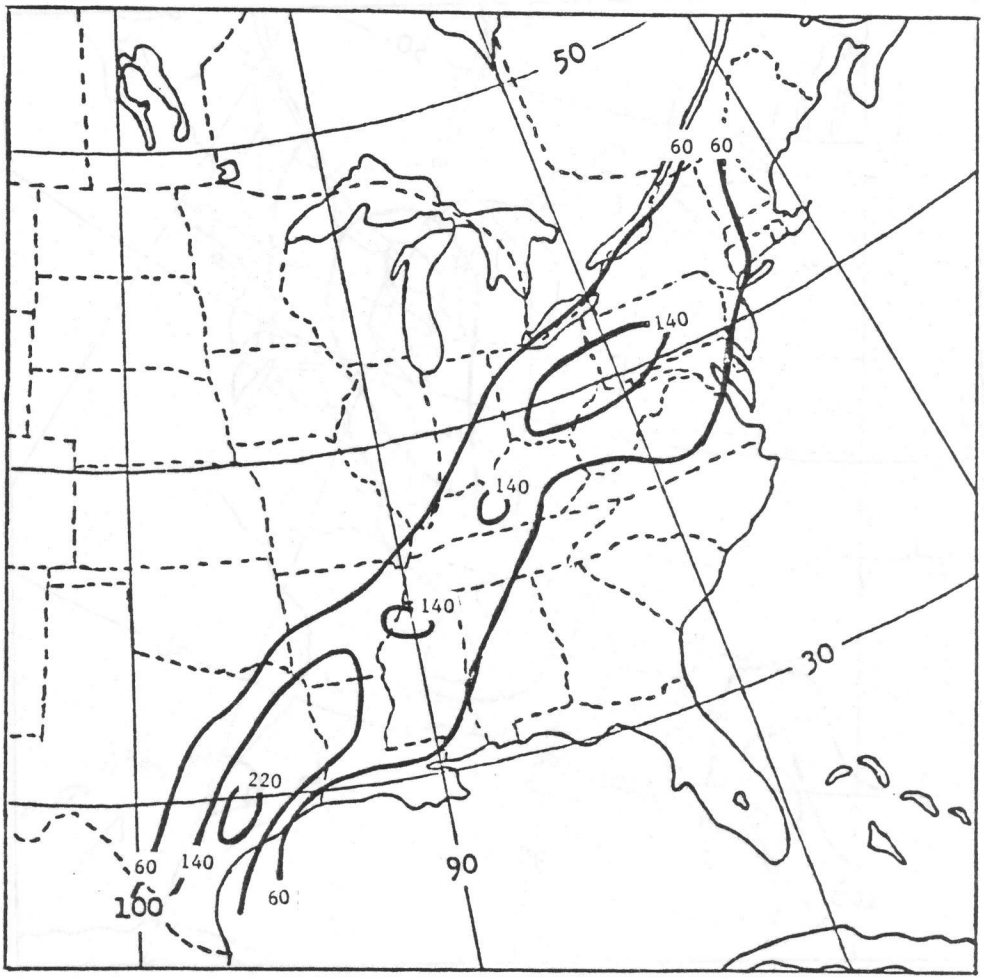

Figure 12. BLM available potential energy term (B), m, 24-h forecast valid 0000 GMT, 3 May 1983.

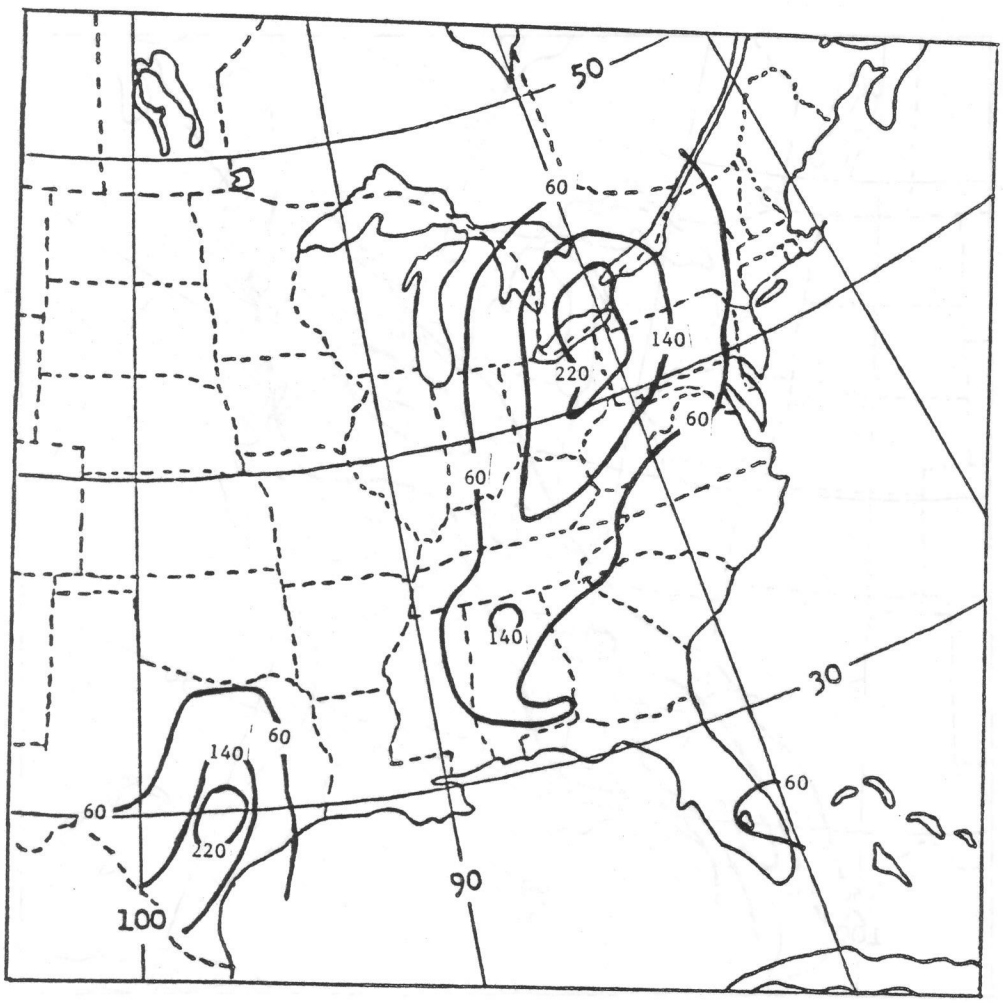

Figure 13. LFM available potential energy term (B), m, 24-h forecast valid 0000 GMT, 3 May 1983.

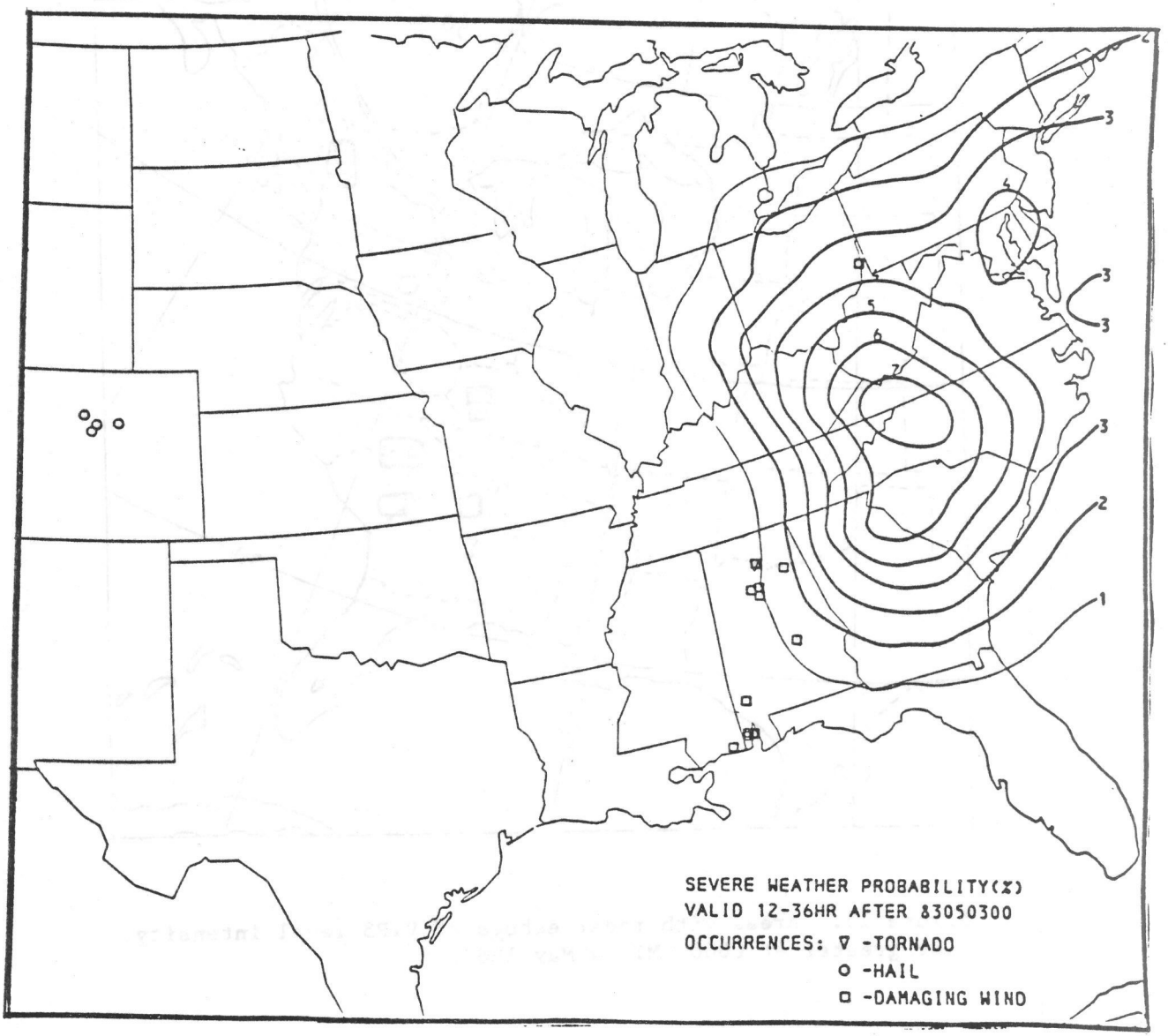

Figure 14. MOS unconditional severe storm probability and severe storm reports during the period 12-36 h after 0000 GMT, 3 May 1983.

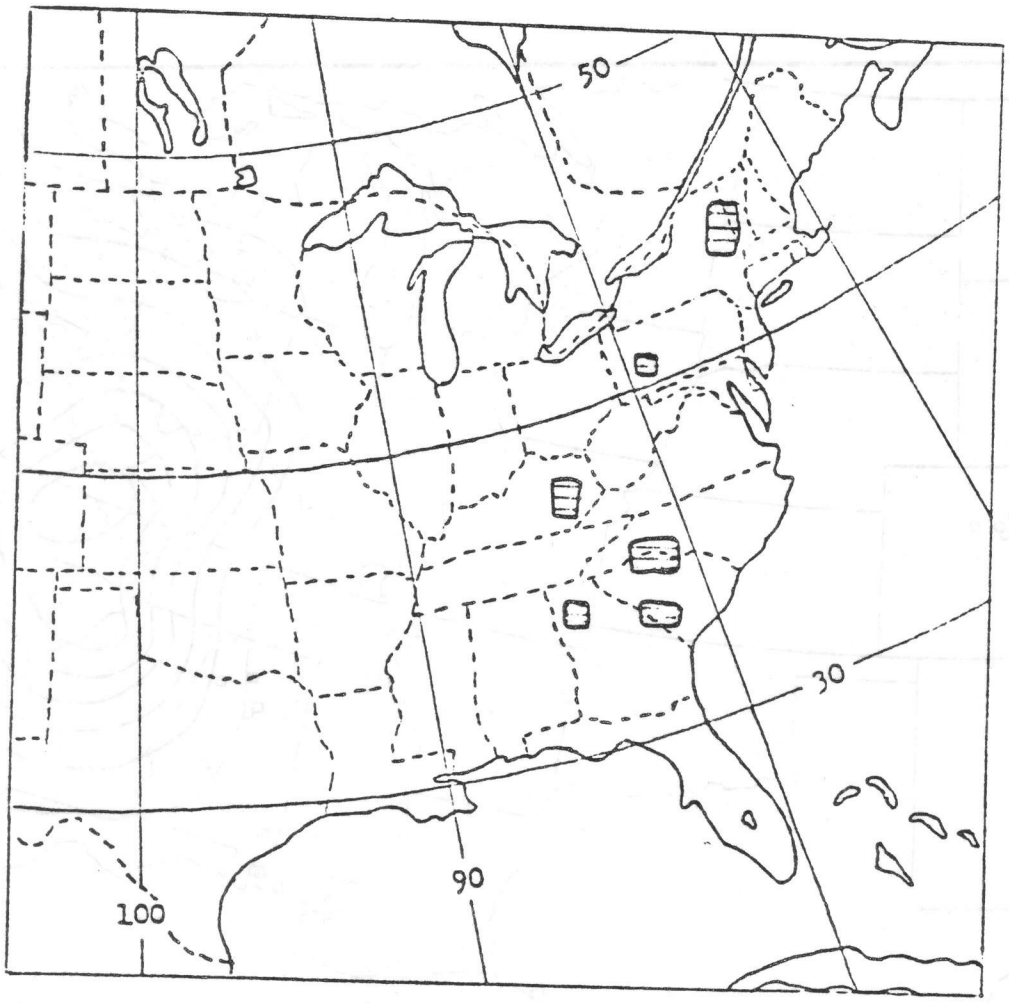

Figure 15. Areas with radar echoes of VIP3 level intensity or greater at 0000 GMT, 4 May 1983.

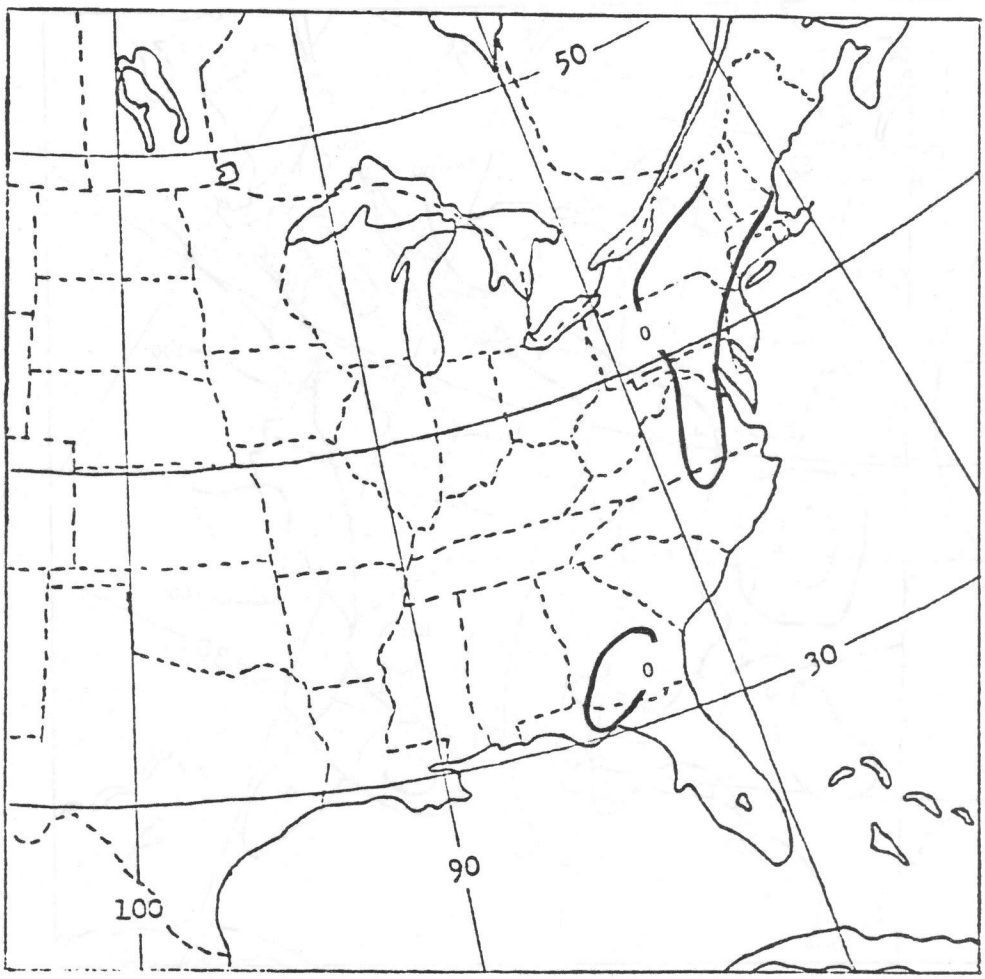

Figure 16. Best lifted index (BLI), K, 24-h forecast valid 0000 GMT, 4 May 1983.

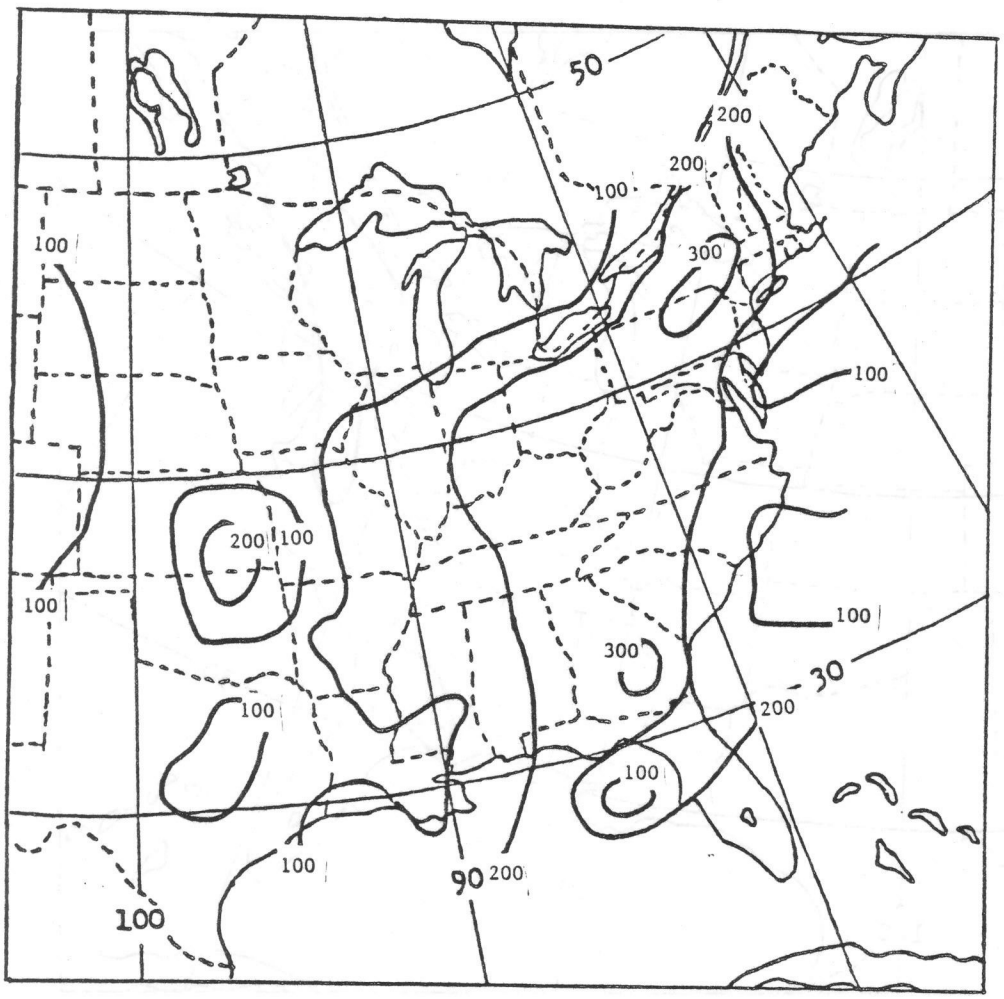

Figure 17. BLM cloud depth (H), mb, 24-h forecast valid 0000 GMT, 4 May 1983.

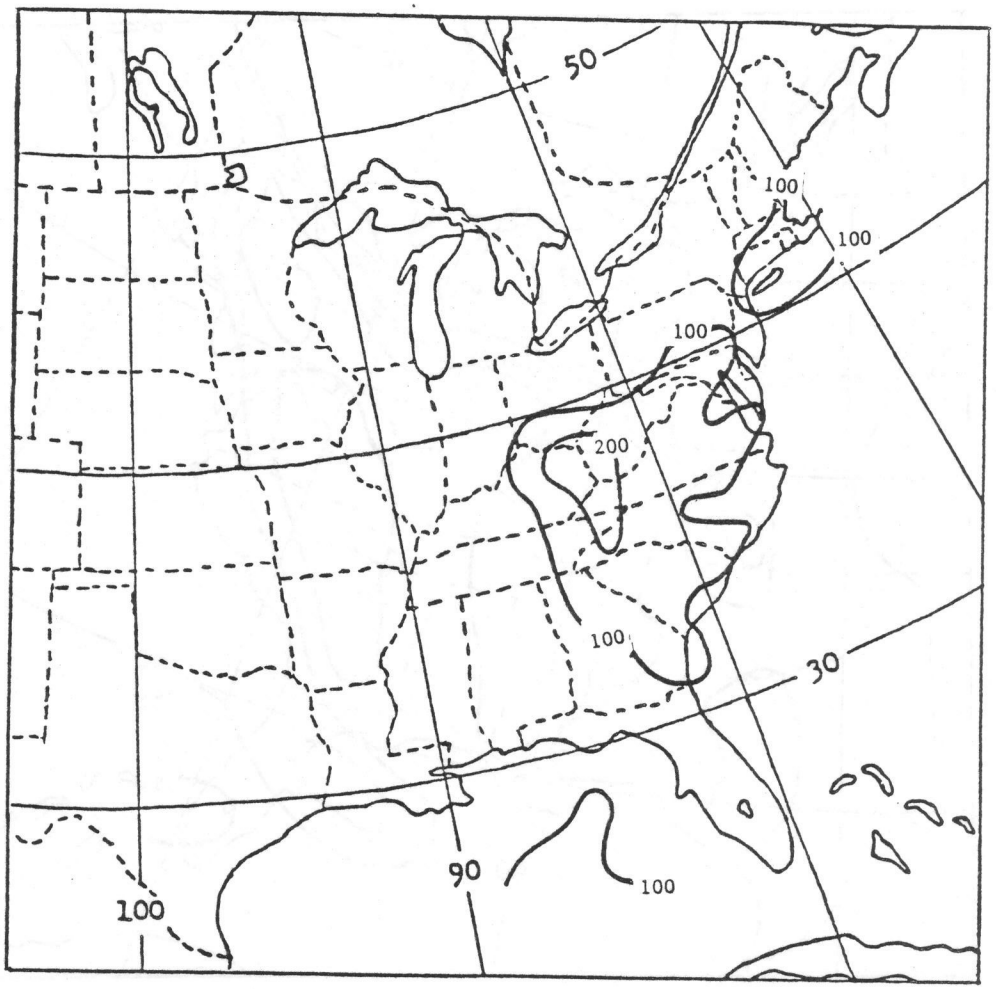

Figure 18. LFM cloud depth (H), mb, 24-h forecast valid 0000 GMT, 4 May 1983.

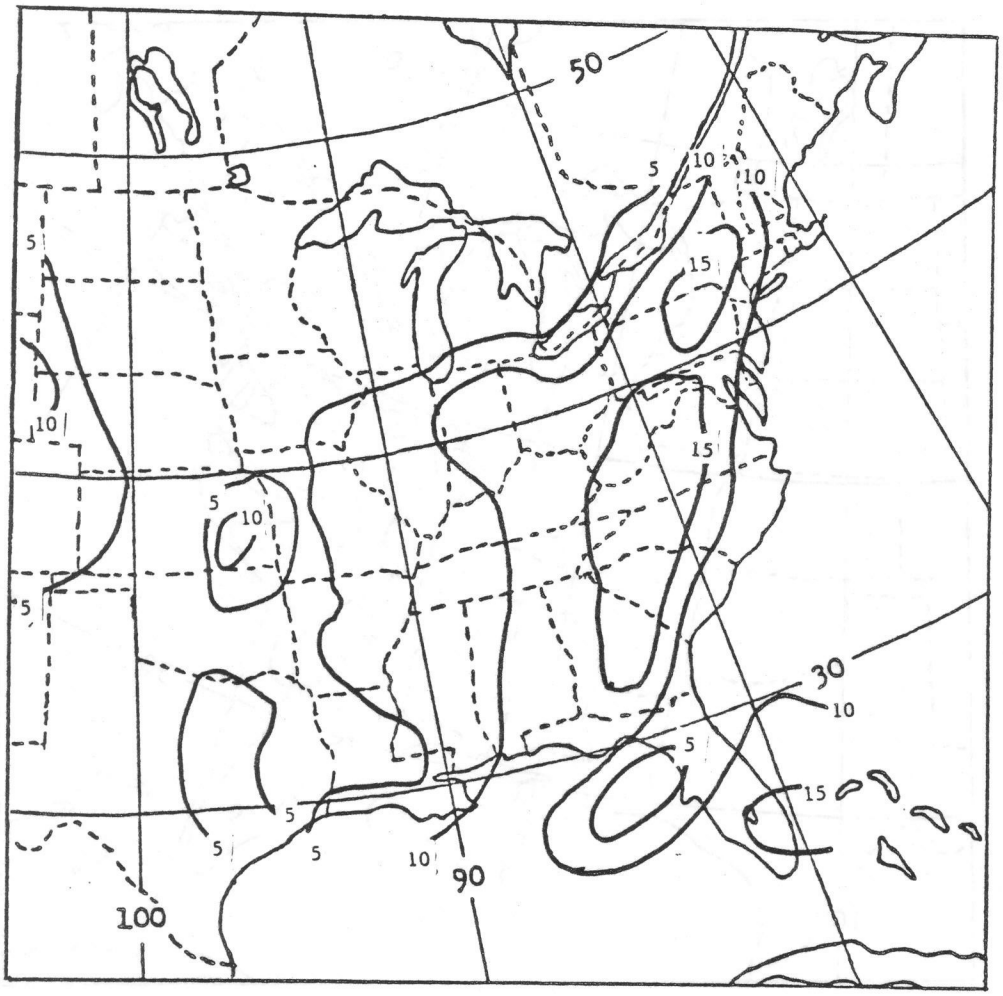

Figure 19. BLM cumulus updraft speed (WMX), m s^{-1}, 24-h forecast valid 0000 GMT, 4 May 1983.

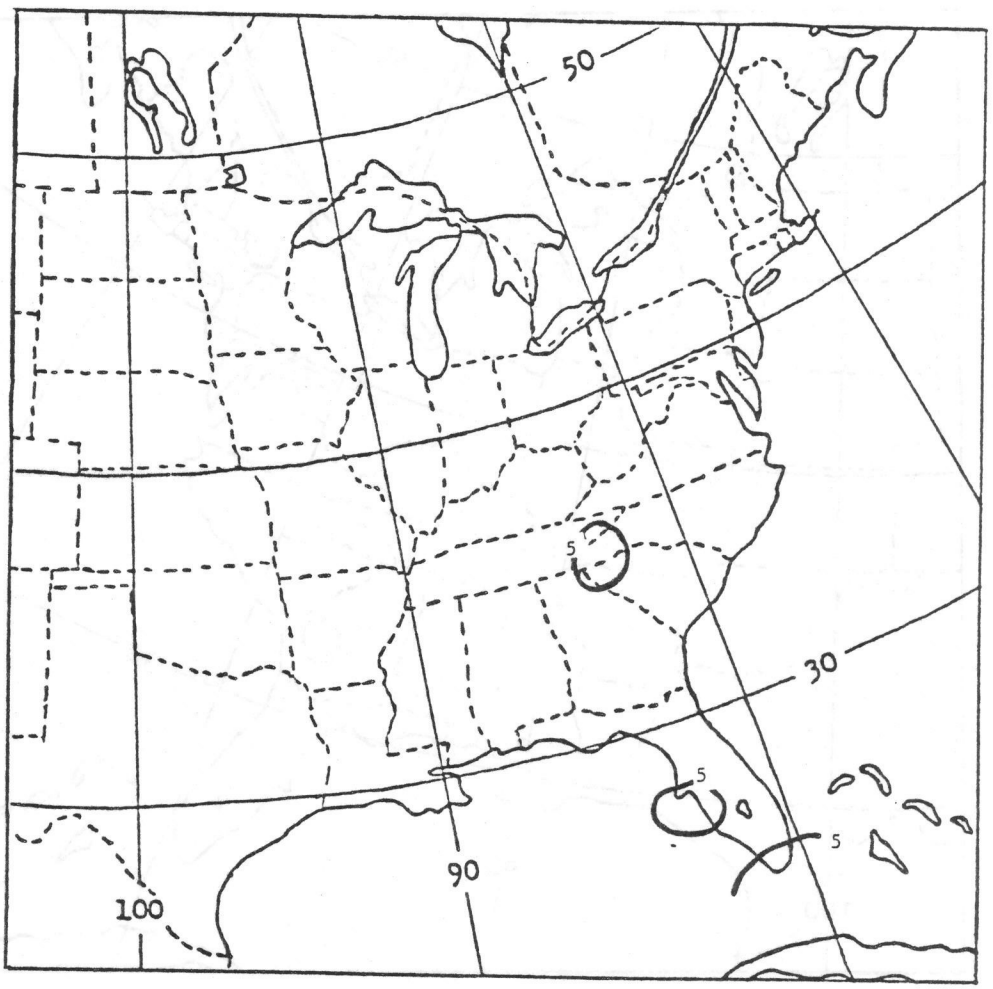

Figure 20. LFM cumulus updraft speed (WMX), m s^{-1}, 24-h forecast valid 0000 GMT, 4 May 1983.

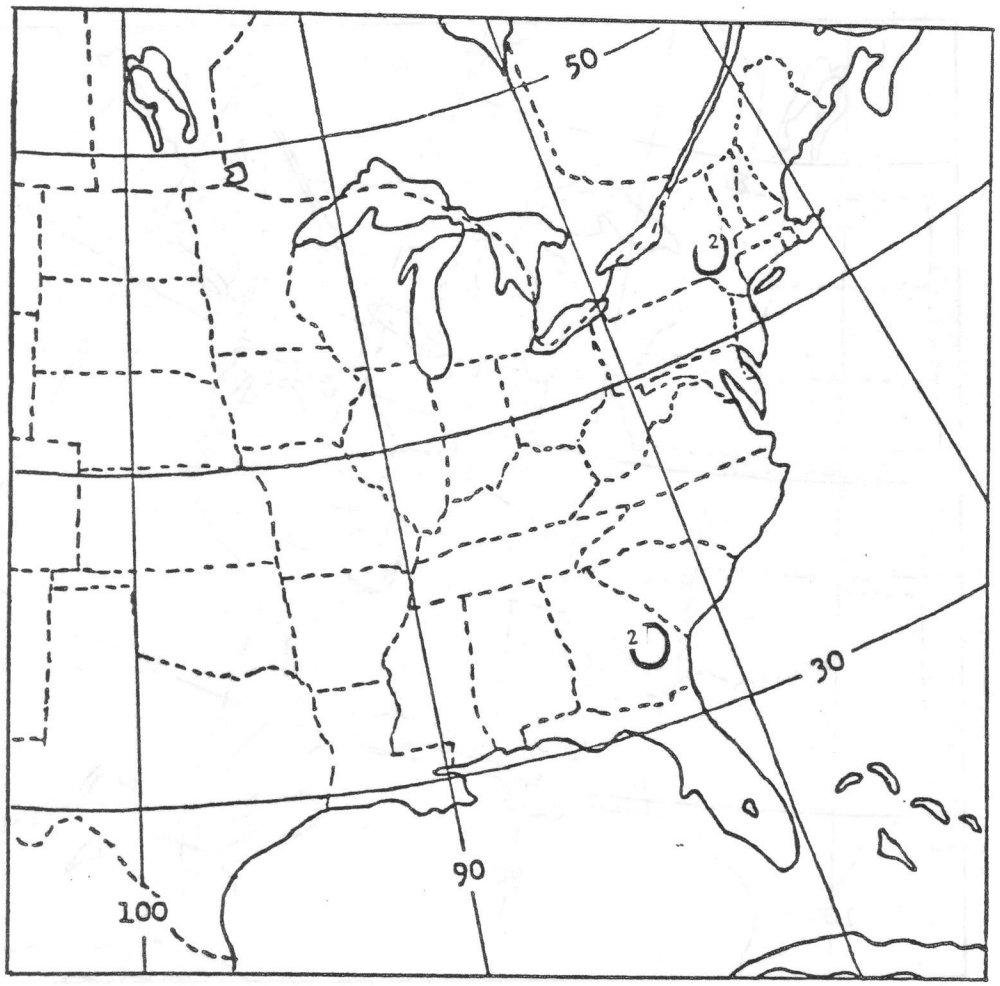

Figure 21. BLM rainout term (RN), mm water, 24-h forecast valid 0000 GMT, 4 May 1983.

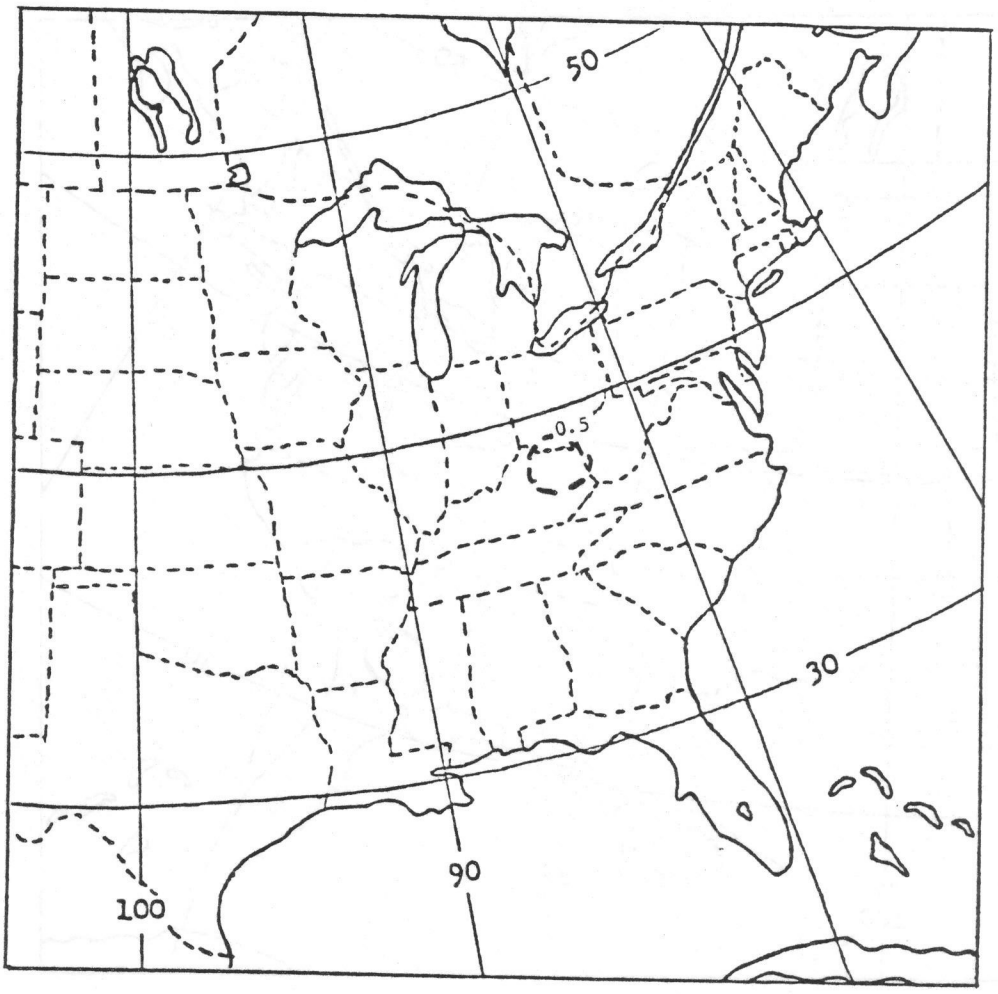

Figure 22. LFM rainout term (RN), mm water, 24-h forecast valid 0000 GMT, 4 May 1983.

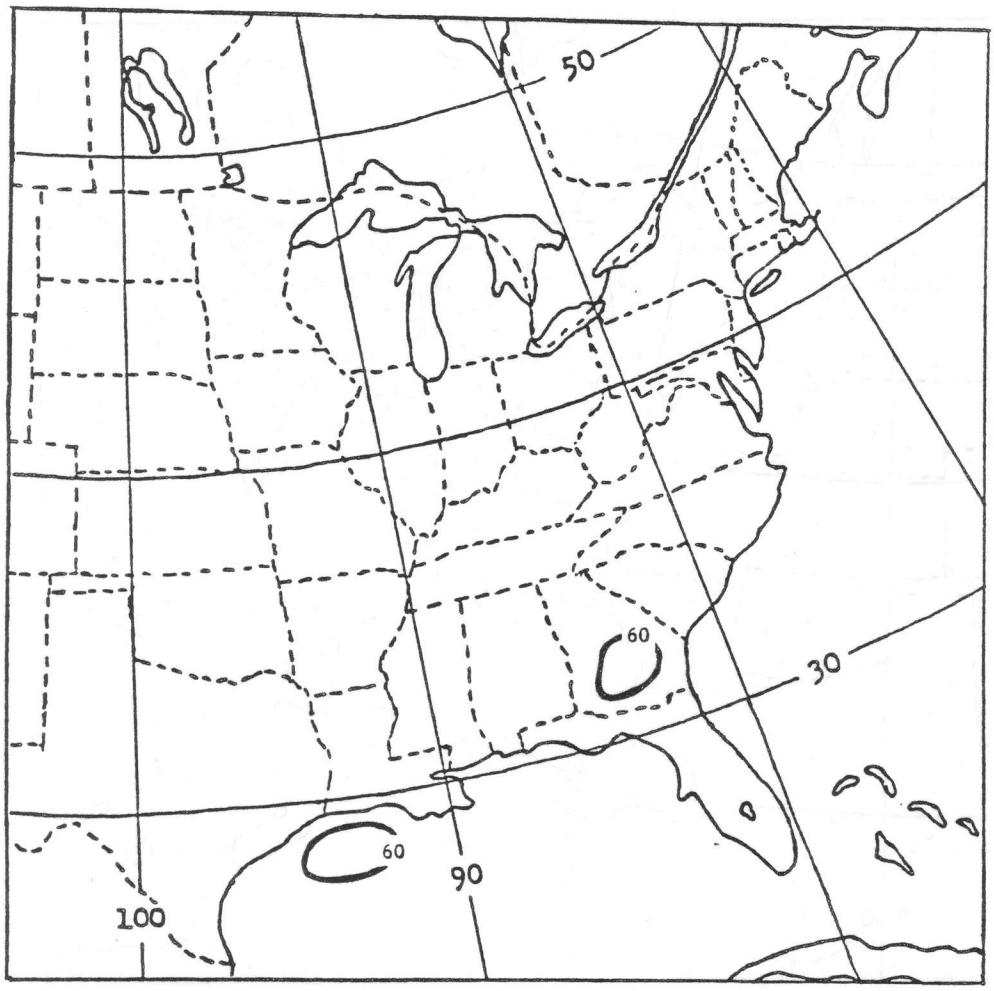

Figure 23. BLM available potential energy term (B), m, 24-h forecast valid 0000 GMT, 4 May 1983.

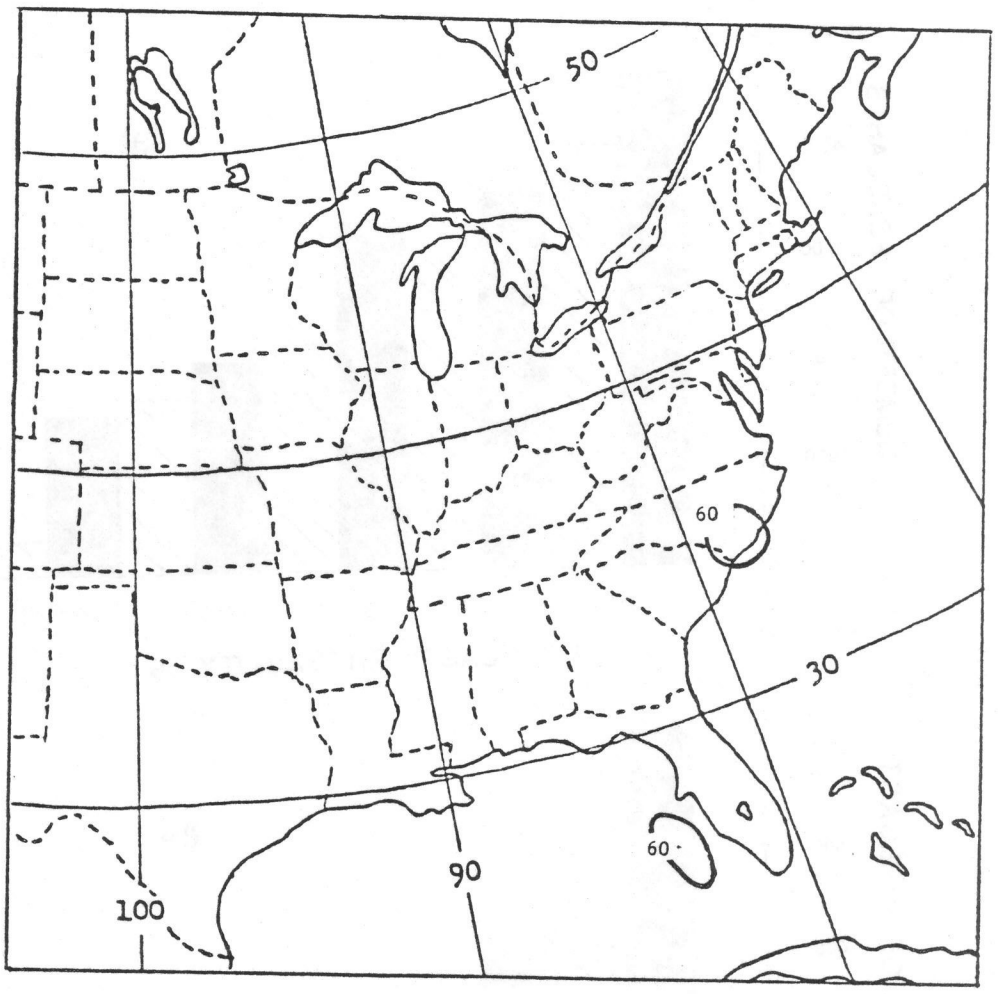

Figure 24. LFM available potential energy term (B), m, 24-h forecast valid 0000 GMT, 4 May 1983.

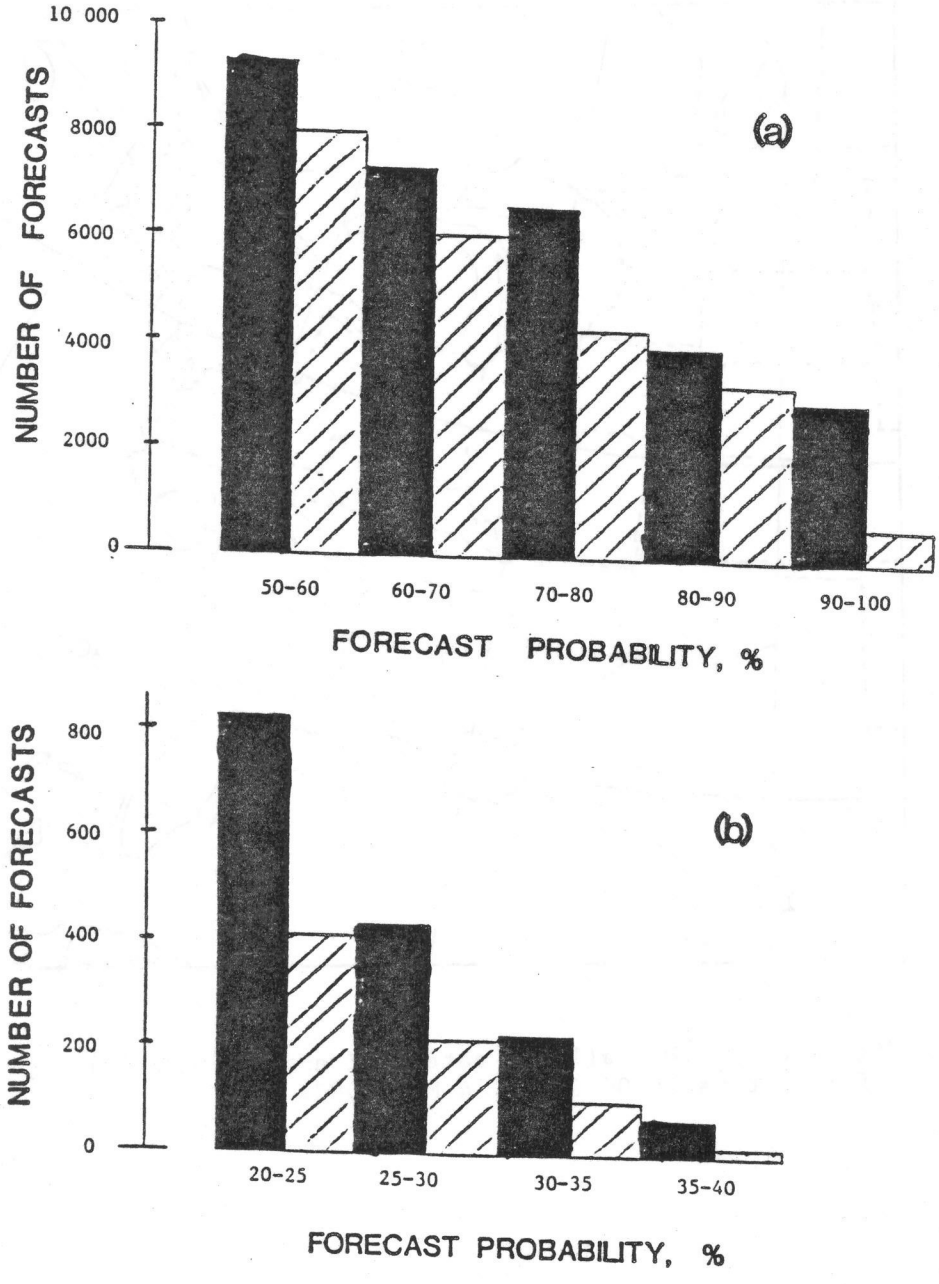

Figure 25. Number of 12-36 h forecasts in each of several probability ranges in the 1982 warm season, for (a) general thunderstorms and (b) severe local storms. Solid blocks are for experimental forecasts, hatched for operational forecasts.

(Continued from inside front cover)

NOAA Technical Memorandums

NWS TDL 42 Some Experiments With a Fine-Mesh 500-Millibar Barotropic Model. Robert J. Bermowitz, August 1971, 20 pp. (COM-71-00958)

NWS TDL 43 Air-Sea Energy Exchange in Lagrangian Temperature and Dew Point Forecasts. Ronald M. Reap, October 1971, 23 pp. (COM-71-01112)

NWS TDL 44 Use of Surface Observations in Boundary-Layer Analysis. H. Michael Mogil and William D. Bonner, March 1972, 16 pp. (COM-72-10641)

NWS TDL 45 The Use of Model Output Statistics (MOS) To Estimate Daily Maximum Temperatures. John R. Annett, Harry R. Glahn, and Dale A. Lowry, March 1972, 14 pp. (COM-72-10753)

NWS TDL 46 SPLASH (Special Program to List Amplitudes of Surges From Hurricanes): I. Landfall Storms. Chester P. Jelesnianski, April 1972, 52 pp. (COM-72-10807)

NWS TDL 47 Mean Diurnal and Monthly Height Changes in the Troposphere Over North America and Vicinity. August F. Korte and DeVer Colson, August 1972, 30 pp. (COM-72-11132)

NWS TDL 48 Synoptic Climatological Studies of Precipitation in the Plateau States From 850-, 700-, and 500-Millibar Lows During Spring. August F. Korte, Donald L. Jorgensen, and William H. Klein, August 1972, 130 pp. (COM-73-10069)

NWS TDL 49 Synoptic Climatological Studies of Precipitation in the Plateau States From 850-Millibar Lows During Fall. August F. Korte and DeVer Colson, August 1972, 56 pp. (COM-74-10464)

NWS TDL 50 Forecasting Extratropical Storm Surges for the Northeast Coast of the United States. N. Arthur Pore, William S. Richardson, and Herman P. Perrotti, January 1974, 70 pp. (COM-74-10719)

NWS TDL 51 Predicting the Conditional Probability of Frozen Precipitation. Harry R. Glahn and Joseph R. Bocchieri, March 1974, 33 pp. (COM-74-10909)

NWS TDL 52 SPLASH (Special Program to List Amplitudes of Surges From Hurricanes): Part Two. General Track and Variant Storm Conditions. Chester P. Jelesnianski, March 1974, 55 pp. (COM-74-10925)

NWS TDL 53 A Comparison Between the Single Station and Generalized Operator Techniques for Automated Prediction of Precipitation Probability. Joseph R. Bocchieri, September 1974, 20 pp. (COM-74-11763)

NWS TDL 54 Climatology of Lake Erie Storm Surges at Buffalo and Toledo. N. Arthur Pore, Herman P. Perrotti, and William S. Richardson, March 1975, 27 pp. (COM-75-10587)

NWS TDL 55 Dissipation, Dispersion and Difference Schemes. Paul E. Long, Jr., May 1975, 33 pp. (COM-75-10972)

NWS TDL 56 Some Physical and Numerical Aspects of Boundary Layer Modeling. Paul E. Long, Jr. and Wilson A. Shaffer, May 1975, 37 pp. (COM-75-10980)

NWS TDL 57 A Predictive Boundary Layer Model. Wilson A. Shaffer and Paul E. Long, Jr., May 1975, 44 pp. (PB-265-412)

NWS TDL 58 A Preliminary View of Storm Surges Before and after Storm Modifications for Alongshore-Moving Storms. Chester P. Jelesnianski and Celso S. Barrientos, October 1975, 16 pp. (PB-247-362)

NWS TDL 59 Assimilation of Surface, Upper Air, and Grid-Point Data in the Objective Analysis Procedure for a Three-Dimensional Trajectory Model. Ronald M. Reap, February 1976, 17 pp. (PB-256-082)

NWS TDL 60 Verification of Severe Local Storms Warnings Based on Radar Echo Characteristics. Donald S. Foster, June 1976, 9 pp. plus supplement. (PB-262-417)

NWS TDL 61 A Sheared Coordinate System for Storm Surge Equations of Motion With a Mildly Curved Coast. Chester P. Jelesnianski, July 1976, 52 pp. (PB-261-956)

NWS TDL 62 Automated Prediction of Thunderstorms and Severe Local Storms. Ronald M. Reap and Donald S. Foster, April 1977, 20 pp. (PB-268-035)

NWS TDL 63 Automated Great Lakes Wave Forecasts. N. Arthur Pore, February 1977, 13 pp. (PB-265-854)

NWS TDL 64 Operational System for Predicting Thunderstorms Two to Six Hours in Advance. Jerome P. Charba, March 1977, 24 pp. (PB-266-969)

NWS TDL 65 Operational System for Predicting Severe Local Storms Two to Six Hours in Advance. Jerome P. Charba, May 1977, 36 pp. (PB-271-147)

NWS TDL 66 The State of the Techniques Development Laboratory's Boundary Layer Model: May 24, 1977. P. E. Long, W. A. Shaffer, J. E. Kemper, and F. J. Hicks, April 1978, 58 pp. (PB-287-821)

NWS TDL 67 Computer Worded Public Weather Forecasts. Harry R. Glahn, November 1978, 25 pp. (PB-291-517)

NWS TDL 68 A Simple Soil Heat Flux Calculation for Numerical Models. Wilson A. Shaffer, May 1979, 16 pp. (PB-297-350)

NWS TDL 69 Comparison and Verification of Dynamical and Statistical Lake Erie Storm Surge Forecasts. William S. Richardson and David J. Schwab, November 1979, 20 pp. (PB80 137797)

NWS TDL 70 The Sea Level Pressure Prediction Model of the Local AFOS MOS Program. David A. Unger, April 1982, 33 pp. (PB82 215492)

NWS TDL 71 A Tide Climatology for Boston, Massachusetts. William S. Richardson, N. Arthur Pore, and David M. Feit, November 1982, 67 pp. (PB83 144196)

NWS TDL 72 Experimental Wind Forecasts From the Local AFOS MOS Program. Harry R. Glahn, January 1984, 60 pp. (PB84-155514)

NWS TDL 73 Trends in Skill and Accuracy of National Weather Service POP Forecasts. Harry R. Glahn, July 1984, 34 pp. (PB84 229053)

NWS TDL 74 Great Lakes Nearshore Wind Predictions from Great Lakes MOS Wind Guidance. Lawrence D. Burroughs, July 1984, 21 pp. (PB85 212876/AS)

NWS TDL 75 Objective Map Analysis for the Local AFOS MOS Program. Harry R. Glahn, Timothy L. Chambers, William S. Richardson, and Herman P. Perrotti, March 1985, 35 pp. (PB85 212884/AS)